Partial Wave Analysis of the Reaction

$\pi^+p \rightarrow \pi^+\pi^-\pi^0\Delta^{++}$ at 7 GeV/c

Max Tabak

Lawrence Berkeley Laboratory

University of California

Berkeley, California

September, 1975

ABSTRACT

An amplitude analysis of the reaction $\pi^+p \rightarrow \pi^+\pi^-\pi^0\Delta^{++}$ at 7 GeV/c has been performed using the isobar model for the 3π system. The 3π mass covers the range .82 to 1.9 GeV. No significant A_1 production can be seen. The spin-parity of the $\omega^*(1700)$ is determined to 3^-. Properties of A_2 and ω^* production are determined and compared with theoretical models. The background is similar to that seen in analyses of charged 3π systems.

This work was done with support from the U.S. Energy Research and Development Administration.

I. Introduction

For several years isobar model analyses of produced charged three pion systems have been available[1,2]. They confirmed the resonant nature of the $A_2(1310)$,but cast doubt on the resonant nature of the $A_1(1070)$. Although a large enhancement appears in the $I(J^P)=1(1^+)$ partial wave,the associated phase does not have the Breit-Wigner behavior associated with a resonance. The respectability of the A_1 is further impaired by the existence of the Deck effect, a combination of t-channel exchange and kinematic accident, which qualitatively explains the A_1 enhancement. On the other hand , a resonant A_1 seems required by many theories, notably the L-excitation quark model,chiral symmetry, and exchange degeneracy[3]. In an attempt to find the "true" A_1 lurking beneath the large Deck background, we studied the reaction

$$\pi^- p \to (\pi^+\pi^-\pi^0)\Delta^{++}, \qquad (1)$$

for which the Deck mechanism is inoperative[4]. Reaction (1) also is suitable for the study of I=0,2 meson final states not accessible to study with charged final states.

By inclusion of information from the Δ^{++} decay and the neglect of double flip amplitudes, we obtain amplitudes free from the continuous ambiguities inherent in density matrix analyses. This allows us, in principle, to determine the phase between natural and unnatural parity exchange amplitudes, and to determine phase variation in a particular three pion partial wave even when

the three pion density matrix is not approximately rank one.

The plan of the report is as follows. In section II we give a brief description of the data and what selections were made. Section III and the appendices describe our formalism. Section IV describes the fitting procedure and the quality of the fits. In Section V, we present our results. Finally, Section VI summarizes the work and poses questions for further study.

II. The Data

These data come from a 700,000 picture exposure of a 7.1 GeV/c π^+ beam on the H_2 filled 82" SLAC-LBL bubble chamber. Experimental details and scanning and measuring efficiencies can be found elsewhere[5,6,7]. There were 85,856 events which fit the reaction

$$\pi^+p \to \pi^+p\pi^+\pi^-\pi^0 \qquad (2),$$

corresponding to a cross section of 2.16 ± .09 mb. Events were selected which had $1.16 \leq M_{\pi^+p} \leq 1.28$ GeV. Ambiguous selections for the correct π^+ to be included in the Δ^{++}, which ranged from 5 to 12% of the sample depending on the recoiling 3π mass, were weighted according to the Δ^{++} Breit-Wigner. In this sample all moments, $\langle Y_L^M \rangle$, of the π^+p decay distributions with $L \geq 3$ are consistent with being zero. We then selected those events which had $|t_{p\Delta}| \leq .8$ (GeV/c)^2 and 3π mass in the interval $.82 \leq M_{3\pi} \leq 1.9$ GeV, giving 12788 events to be analyzed.

To study the amount of pollution from higher N^*'s we consider the region where their effect is expected to be maximal: large $|t_{p\Delta}|$ and $M_{3\pi}$. Figure 1 shows the $\Delta^{++}\pi^-$ and $\Delta^{++}\pi^0$ mass distributions, where the diamonds represent the N^{*0}'s and the histogram gives the N^{*++}'s, for $1.7 \leq M_{3\pi} \leq 1.8$ GeV and $.35 \leq |t_{p\Delta}| \leq .8$ $(GeV/c)^2$. Notice that both graphs peak sharply at low mass. However, the only known N^* in this region has isospin 1/2, so the N^{*++} signal here must be a reflection of some other feature of the data. Similarly, we argue that much of the N^{*+} signal is also a reflection. Consequently, we estimate the total N^* pollution as < 70 events in this 883 event sample[8]. Because what N^* signal exists is distributed among many N^*'s, none of which dominates the cross section in its region, the effect of exclusions (biased angular distributions and greatly decreased statistics) is worse than the malady that they would seek to cure. Therefore, no cuts were performed on the data.

III. Formalism

For reaction (1) we define the production amplitude $T^{J^P M n}_{\lambda_\Delta,\lambda_p}(M_{3\pi},t_{p\Delta})$, where $J,P,M_{3\pi}$, and $t_{p\Delta}$ are the angular momentum of the produced three pion system, its parity, its mass, and momentum transferred squared between the incoming proton and the outgoing Δ^{++}, respectively. n labels the set of 3-pion

quantities: {isospin, isobar, orbital angular momentum between isobar and odd pion}, and will be more fully described in Appendix A. $M(\lambda_p,\lambda_\Delta)$ is the z-component of spin of the three pion system (incoming proton, outgoing Δ) along the vector $\vec{C}$ ($\vec{C}'$) in the three pion (Δ) rest frame. C_μ (C_μ') is the four vector independent of $M_{3\pi}$ (M_Δ), orthogonal to the four-momentum of the produced meson (baryon) system, and whose spatial components lie in the production plane. In the situation that $|t_{p\Delta}| << s$, we have:

$$\vec{C} = \vec{q}_\pi + \frac{t-m_\pi^2}{2s}(\vec{q}_p + \vec{q}_\Delta) \qquad (3),$$

where $\vec{q}_\pi$ ($\vec{q}_p$, $\vec{q}_\Delta$) is the momentum of the pion (proton, Δ) in the rest frame of the 3 pion system. And,

$$\vec{C}' = \vec{q}_p' + \frac{t-m_p^2}{2s}(\vec{q}_\pi' + \vec{q}_{3\pi}') \qquad (4),$$

where $\vec{q}_p'$ (q_π', $\vec{q}_{3\pi}'$) is the momentum of the incoming proton (pion, outgoing three pion system) in the Δ rest frame. In both cases we take the $\vec{Y}$ axis as the normal to the production plane:

$$\vec{Y} = \vec{q}_p \times \vec{q}_\Delta \qquad (5).$$

These choices for quantization axes are motivated by the vector dominance model of Cho and Sakurai[9] as extended by Wagner[10], which predicts helicity conservation in this frame. This model has been successful in describing the production of both vector mesons and diffractive meson and N^* systems. Therefore, this frame was adopted with the hope that its use would reduce the number of parameters required to fit the data and as a test of these dynamical models. On the other hand, for most of our

kinematic range this coordinate system is within 30° of the t-channel frame for which approximate helicity conservation has been observed in similar analyses of charged three pion systems[1,2]. This fact weakens our ability to test these models, while making it likely that we can't be too far wrong in our choice of coordinate systems.

The dependence of the production amplitude under rotations on the baryon spins is of the form: $|1/2\rangle\times|3/2\rangle$. We decompose this Kronecker product as:

$$T^{J^P M n}_{\lambda_\Delta,\lambda_p} = \sum_{s,\mu} \langle 1/2\ \lambda_p\ S\ \mu | 3/2\ \lambda_\Delta\rangle\ T^{J^P M n}_{S,\mu} \sqrt{(2S+1)/2} \qquad (6).$$

If S is restricted to 1, we have the so-called class A predictions of the quark model[11]: those which depend only on additivity. That is, the meson-baryon scattering amplitude is the sum of constituent quark-quark scatterings. Since a single quark can experience only single flip and both proton and Δ^{++} have the same orbital angular momentum in the symmetric quark model classification scheme[12], the baryon current must behave as a spin-one object under rotations. Similar predictions come from a dipole coupling model[13] or for natural exchange alone (see below) the venerable Stodolsky-Sakurai model[14]. These models have been successful in describing the production of the delta isobar when the associated meson system was either a π, K, ρ, $K^*(890)$, or $\omega(780)$.

This decomposition of the production amplitude is also useful

in imposing parity constraints. By reflecting in the production plane, we obtain:

$$T^{J^P Mn}_{\lambda_\Delta,\lambda_p} = P(-1)^{J-M-\lambda_\Delta-\lambda_p-1}\, T^{J^P-Mn}_{-\lambda_\Delta,-\lambda_p} \qquad (7).$$

The decomposed amplitudes obey the following rule:

$$T^{J^P Mn}_{S\mu} = P(-1)^{J-M+S-\mu-1}\, T^{J^P-Mn}_{S\mu} \qquad (8).$$

This restriction is built into our formalism as follows. If we define

$$Y_m = P(-1)^{J-|M|-1} \qquad (9),$$

for the meson vertex and

$$Y_B = (-1)^{S-|\mu|} \qquad (10)$$

for the baryon vertex, then a new amplitude can be written which manifests parity conservation for the production reaction:

$$\epsilon(\mu)\epsilon(M)\eta_B[(T^{J^P Mn}_{S\mu}+\eta_M Y_m T^{J^P-Mn}_{S\mu}) + \eta_B Y_B(T^{J^P Mn}_{S-\mu}+\eta_M Y_m T^{J^P-Mn}_{S-\mu})]$$

(11),

where the quantities η_M and η_B can take the values ± 1, and

$$\epsilon(\mu) = \sqrt{2}/4 \text{ , for } \mu=0$$
$$= \sqrt{2}/2, \text{ for } \mu\neq 0 \qquad (12).$$

This expression , denoted by $T^{J^P|M|n\eta}_{S|\mu|}$, vanishes unless $\eta_M=\eta_B=\eta$. to the order (1/s), $\eta=+1(-1)$ corresponds to exchange in the t-channel of objects of natural (unnatural) parity[15].

The amplitude for a meson system of quantum numbers J,P,M,n to decay into three pions, denoted by G^{JPMn}, is given in reference 16. We sketch a derivation in Appendix A. The Δ^{++} decay amplitude is given by

$D^{*3/2}_{\lambda_\Delta,\lambda_{p'}}(\alpha,\beta,\gamma)$, where $\lambda_{p'}$ is the helicity of the decay proton and

α,β,γ are the Euler angles which rotate the outgoing proton from $\hat{C}$ to its direction. The total amplitude for a particular event for given incoming proton spin, λ_p, and outgoing proton helicity, $\lambda_{p'}$, is then of the form:

$$T_{\lambda_p\lambda_{p'}} = \sum_{S,\mu} H_{S,\mu,\lambda_p,\lambda_{p'}} \sum_{J^P,M,n} G^{J^PMn}\, T^{J^PMn}_{S,\mu} \qquad (13),$$

where,

$$H_{S,\mu,\lambda_p,\lambda_{p'}} = \sqrt{(2S+1)/2}\,(1/2\ \lambda_p\ S\ \mu|3/2\ \lambda_\Delta)\ D^{*1/2}_{\lambda_\Delta,\lambda_\mu} \qquad (14).$$

For a particular choice of J^P,n,S,λ_p, and $\lambda_{p'}$ consider the partial sum:

$$h = \gamma(M)\gamma(\mu)[T^M_\mu G^M H_\mu + T^{-M}_\mu G^{-M} H_\mu + T^{-M}_{-\mu} G^{-M} H_{-\mu} + T^M_{-\mu} G^M H_{-\mu}]$$

(15),

$$\text{where } \gamma(M) = 1/2 \text{ for } M=0, \quad = 1 \text{ for } M\neq 0. \qquad (16)$$

In terms of amplitudes of definite η, we have:

$$h = \frac{\gamma(M)\gamma(\mu)}{4\epsilon(M)\epsilon(\mu)}[(T^+ + T^-)(Y_B G^M H_{-\mu} + Y_M G^{-M} H_\mu) + (T^+ - T^-)(Y_M Y_B G^{-M} H_{-\mu} + G^M H_\mu)] \qquad (17),$$

$$= \frac{\gamma(M)\gamma(\mu)}{4\epsilon(M)\epsilon(\mu)}[T^+(G^M + Y_M G^{-M})(H_\mu + Y_B H_{-\mu}) + T^-(-iG^M + iY_M G^{-M})(-iH_\mu + iY_B H_{-\mu})] \qquad (18).$$

Consequently,

$$T_{\lambda_p,\lambda_{p'}} = \sum_{S,\mu} \frac{\gamma(\mu)}{2\epsilon(\mu)}[(H_{-\mu} + Y_B H_\mu) \sum_{J^P|M|n} T^{J^P|M|n}_{S,\mu} \frac{\gamma(M)}{2\epsilon(M)}(G^M + Y_M G^{-M}) + i(H_{-\mu} - Y_B H_\mu) \sum_{J^P|M|n} T^{J^P|M|n}_{S,\mu} - \frac{i\gamma(M)}{2\epsilon(M)}(G^M - Y_M G^{-M})]$$

(19).

Schematically, we have

$$T_{\lambda_p,\lambda_{p'}} = \sum_{S|\mu i} (H^{+}_{S,|\mu i} \vec{T}^{+}_{S,|\mu i} \vec{G}^{+} + H^{-}_{S,|\mu i} \vec{T}^{-}_{S,|\mu i} \vec{G}^{-}) \qquad (20),$$

The spin averaged intensity is:

$$I = \sum_{\substack{S|\mu i|\eta \\ S'|\mu i'|\eta'}} (\vec{T}\cdot\vec{G})^{*}_{S,|\mu i,\eta} A^{S,|\mu i\eta}_{S',|\mu i'\eta'} (\vec{T}\cdot\vec{G})^{S',|\mu i',\eta'} \qquad (21),$$

where A is a matrix calculated in Appendix B.

IV Fitting

The programs employed were extensively modified versions of programs used for isobar model analyses of low energy $\pi N \to N\pi\pi$[17] formation reactions and $\pi^+ p \to (\pi^+\pi^+\pi^-)p$ [1]. There are three major programs and a number of subsidiary ones, which in various versions run on large CDC and IBM computers. The first program in the string, LTRI, computes the G functions and the A matrix (see section III and the appendices) for both the data and Monte Carlo generated events. Roughly, 10–20 Monte Carlo events were generated for each real event. The Monte Carlo events were input to the program KREBS which calculated normalization integrals. If $\vec{G}^{+}$ and $\vec{G}^{-}$ are vectors of G-functions for natural and unnatural exchange, respectively, and

$$K_{+} = \int \vec{G}^{+}(\vec{G}^{+})^{\dagger} \text{ and } K_{-} = \int \vec{G}^{-}(\vec{G}^{-})^{\dagger} \qquad (22),$$

where the integrals are over three pion phase space and † denotes Hermitian adjoint, then we have for the cross section

$$\sigma = \sum_{i} (\vec{T}^{+}_{i})^{\dagger} \cdot K_{+} \cdot \vec{T}^{+}_{i} + \sum_{j} (\vec{T}^{-}_{j})^{\dagger} \cdot K_{-} \cdot \vec{T}^{-}_{j} \qquad (23),$$

where the sums are over p-Δ labels and all possible inner products are to be performed. The K matrices can also be calculated with a numerical integration over the Dalitz plot, but the Monte Carlo events were also useful for comparisons of the fits with the data. The C-vectors, A and K matrices were input for the program PWA3PI, a user function for the general purpose fitting system, OPTIME[18]. Using a modified Newton-Raphson technique, OPTIME maximized the log likelihood given by

$$\ln L = \sum_{i=1}^{N} \ln(I^i) - N\sigma \qquad (24),$$

where N is the number of events, I (eq. 21) is the probability for a given event and σ is given by eq. 23, in which the T's act as fitting parameters. This form of likelihood function automatically normalizes our amplitudes to the number of experimentally observed events. A quoted partial wave cross section is then given by $|T_i|^2 K_{ii}$, where T_i is a particular element of a particular $\vec{T}$ vector and K_{ii} is the associated diagonal element of the matrix K.

The data were binned in the three pion mass, $M_{3\pi}$, and momentum transferred squared, $t_{p\Delta}$, between proton and Δ^{++} with approximately 500 events/bin. For mass dependent fits, two t intervals were used: $0 \le |t| \le .35$ and $.35 \le |t| \le .8$ $(GeV/c)^2$ (hereafter, low t and high t). t-dependent fits were performed in two mass regions: $1.2 \le M_{3\pi} \le 1.4$ GeV (A_2 region) and $1.6 \le M_{3\pi} \le 1.8$ GeV (ω^* region). Since the A_2 and ω^* amplitudes vary considerably over 200 MeV, we included factors of $(E_0 - M_{3\pi} - i\Gamma/2)^{-1}$ in the fitting

parameters, where the central mass and width had been determined in the mass dependent fits. This procedure was also applied to mass dependent fits. Across the peak of the A_2 this improved the log-likelihood by 50 for equal numbers of parameters, although individual partial wave cross sections were, within errors, unchanged.

For a list of meson partial wave quantum numbers allowed at each $M_{3\pi}$ see Table I. We neglected amplitudes which had helicity changes of more than one unit at either meson or baryon vertex. At the highest masses, this still gives, counting both meson and baryon quantum numbers, 473 real parameters. This wealth of parameters is associated, unfortunately, with a paucity of events. Consequently, we adopted the following fitting strategy: First, we varied only those waves which were present in the charged 3π system as determined by previous analyses[1,2] for both I=0 and I=1 amplitudes, and only S=1 amplitudes at the p-Δ vertex. Then, in succeeding fits, we added parameters with the aim of significantly increasing both the likelihood and the energy continuity of the solutions. We rejected those parameters which did not meet these criteria. This procedure was iterated until the major waves stopped changing. Not only did we vary the set of waves, but we also tried multiple starting points for a given set: usually the fits converged to the same solution. The results presented here are those of our highest likelihood solutions (for $M_{3\pi} \geq 1.2$ GeV we use

those where the resonances have energy dependent parametrization) but share major features with earlier fits.

We were guided in our selection of parameters by certain moments of the Δ^{++} decay distribution. If (p_x,p_y,p_z) is a unit vector in the direction of the outgoing proton in the Δ^{++} rest frame, we have, using the K matrices as metrics, the following relations between the $T^{\eta}_{S\mu l}$ and certain moments (see Appendix B):

$$W_+ \equiv \langle 5p_y^2 - \frac{4}{3}\rangle = |\vec{T}^+_{11}|^2 + \frac{1}{3}|\vec{T}^-_{00}|^2 + \frac{2}{3}|\vec{T}^-_{21}|^2 - \frac{1}{3}|\vec{T}^+_{21}|^2 + \frac{2}{\sqrt{3}}\mathrm{Re}(\vec{T}^{-\dagger}_{11}\cdot\vec{T}^-_{21}) \quad (25)$$

$$W_- \equiv \langle 5p_x^2 - \frac{4}{3}\rangle = |\vec{T}^-_{11}|^2 + \frac{1}{3}|\vec{T}^-_{00}|^2 - \frac{1}{3}|\vec{T}^-_{21}|^2 + \frac{2}{3}|\vec{T}^+_{21}|^2 + \frac{2}{\sqrt{3}}\mathrm{Re}(\vec{T}^{+\dagger}_{11}\cdot\vec{T}^+_{21}) \quad (26)$$

$$W_0 \equiv \langle 5p_z^2 - \frac{4}{3}\rangle = |T^-_{10}|^2 + \frac{1}{3}|\vec{T}^-_{00}|^2 + \frac{2}{3}|\vec{T}^-_{21}|^2 + |\vec{T}^+_{20}|^2 + \frac{2}{3}|\vec{T}^+_{21}|^2 - \frac{2}{\sqrt{3}}\mathrm{Re}(\vec{T}^{-\dagger}_{11}\cdot\vec{T}^-_{21} + \vec{T}^{+\dagger}_{11}\cdot\vec{T}^+_{21}) \quad (27)$$

Note that if only S=1, i.e. quark model, amplitudes contribute, W_+ gets contributions from natural exchange only, while unnatural exchange contributes to W_0 and W_-. However, the total amounts of natural and unnatural exchange can be determined from the meson vertex alone. These independent measurements of naturality contributions give a direct test of the hypothesis: S=1 only. In fact, large amounts of S=2 were required. A comparison of the W_i as determined from the fits with those from the

moments as a function of $M_{3\pi}$ for low and high t is shown in figures 2-4.

In figures 5-10 we compare the fit at high t for the mass interval $1.6 \leq M_{3\pi} \leq 1.7$ with various projections of the data. χ^2's of 30 for 20 degrees of freedom were typical. This can be compared with the results of a low energy $\pi N \rightarrow \pi\pi N$ isobar model analysis[19] which had sufficient statistics to simultaneously bin in all kinematic variables. For one dimensional projections they had typically, $\chi^2/ND = 20/10$, while their 4-dimensional χ^2/ND were typically 225/225. This illustrates several points concerning isobar model likelihood fits. First, they can't track rapid fluctuations unless they are put in by hand. For instance, on figure 10 the ρ^0 signal is well fit, while the bump near the f^0 mass is much narrower than the f^0 is thought to be. Second, these model fits average over regions in the total phase space to maximize the agreement between model prediction and local event density. This means that they are less sensitive to measurement errors and statistical fluctuations than analyses where this one-to-one correspondence between the events and the model is lost. Thus, if these models are to be improved to better understand the underlying dynamics, we must drastically improve statistics (so that failures of the model can be separated from the statistical jitter) and find ways to propagate measurement errors to the fitted amplitudes.

V. Results[20]

Figure 11 shows the mass distributions for both t intervals. The peak at $M_{3\pi} \approx 1.3$ GeV is taken up by the $IJ^P = 1\ 2^+$, A_2, and that at $M_{3\pi} \approx 1.7$ GeV by the $\omega^*(1700)$ found earlier in its (3π) and (5π) decays[21,22]. This analysis has determined that the IJ^P assignment of this state is $0\ 3^-$. A fit with a Breit-Wigner distribution to the points for the A_2 cross section at low t gives a mass of (1.298 ± 0.008) GeV and a width of (0.122 ± 0.012) GeV. Figures 12 and 13 give the phase of the $T^{|M|\eta}_{S\mu}$ $[I(J^P\text{isobar})] = T^{0^-}_{10}$ $[1(2^+\rho)]$, $T^{1^+}_{11}$ $[1(2^+\rho)]$, $T^{0^+}_{20}$ $[1(0^-\epsilon)]$, $T^{0^+}_{20}$ $[1(2^-\epsilon)]$ amplitudes relative to the $T^{0^+}_{20}$ $[1(2^-f)]$ amplitude in the A_2 region. The A_2 phases are modulo $\tan^{-1}[.061/(1.298 - M_{3\pi})]$. The large $T^{0^-}_{10}$ $[1(2^+\rho)]$ shows nice Breit-Wigner phase behavior, while the smaller $T^{1^+}_{11}$ $[1(2^+\rho)]$ although consistent with Breit-Wigner behavior is much less stable. Integrating the A_2 Breit-Wigner gives a production cross section of $(53 \pm 7)\ \mu b$ for $|t| \leq .8\ (GeV/c)^2$.

A Breit-Wigner fit to the ω^* mass plot at high t gives a mass of $(1.669 \pm .011)$ GeV and a width of (0.173 ± 0.019) GeV. Integrating this gives a production cross section of $(33 \pm 12)\mu b$ for $|t| \leq .8$ $(GeV/c)^2$. Figures 14 and 15 give the phases of the $T^{0^-}_{10}$ $[0(3^-\rho)]$, $T^{0^-}_{11}$ $[0(3^-\rho)]$, $T^{0^+}_{20}$ $[1(0^-\epsilon)]$, $T^{0^+}_{20}$ $[1(2^-f)]$, relative to the $T^{0^+}_{20}$ $[1(2^-\epsilon)]$ in the high t interval. The ω^* phases are modulo $\tan^{-1}[.086/(1.669 - M_{3\pi})]$. The combination of small cross sections, N^* pollution, absence of large constant background waves

and averaging over large t-intervals makes obtaining reliable ω° phases difficult. The situation is further complicated by the fact that the ω° branching ratio into T_{10}^{0-} and T_{11}^{0-} changes across the peak of the distribution. That is, the ω° polarization is constant across the bump, but the associated Δ polarization changes. This is reflected in the W_0 and W_- moments which have spikes at slightly different masses (figures 2,3). Nevertheless, the Breit-Wigner shape of the mass plot, together with a mass and width comparable to that of the g-meson, makes a resonance interpretation plausible if not certain.

Both the A_2 and the ω° are produced dominantly by unnatural exchange as predicted by Fox and Hey[23], and in agreement with recent experimental results[24] on the reaction $\pi^+n \to (\pi^+\pi^-\pi^0)p$. In fact, semi-inclusive duality[25] predicts the following scaling law for the ratio R of natural to unnatural exchange:

$$R \sim (m^2)^{(2a_N(t)-2a_U(t))} \qquad (28),$$

where m is the resonance mass, and a_N and a_U are the natural and unnatural exchange trajectories. Taking $a_N - a_U$ as 0.5[26](this value comes from effective trajectory fits to density matrix elements of the reaction $\pi^+p \to \Delta^{++}\omega$ and thus includes the effect of cuts and ill understood backgrounds, but agrees with the theoretical idea of π-B exchange degeneracy) and using the value $R_\omega^{26,27} = .8 \pm .07$, we obtain the predictions $R_{A_2} = 0.29 \pm 0.03$ and $R_\omega^\circ = 0.18 \pm 0.02$. This is in fine agreement with our observed

ratios of $R_{A_2} = 0.34 \pm .03$ and $R_{\omega}^{\circ} = 0.24 \pm 0.04$. However, this agreement may be fortuitous as we shall see when the results of the t-dependent fits are presented.

There are marked differences in the production mechanisms between the natural spin parity resonances and the unnatural spin parity background. Whereas we have seen that the resonances are produced dominantly by unnatural exchange, the background is produced by natural exchange. Figures 16a,b show the ratios of unnatural to natural exchange for the background amplitudes. The non-quark amplitudes $T^{[\mu\mu]\eta}_{\Sigma\mu\lambda}$ are not required for the resonances, but they dominate the background. This is shown in figures 17a,b. Apparently this background cannot be produced via a Deck or multiperipheral mechanism since the p-Δ coupling is unlike that found in other natural exchange dominated reactions. Furthermore, the background is helicity conserving to the level of 10% in our coordinate system as figures 18a,b bear out.

The background is shared by many partial waves. In figures 19-22 we show the strongest of these. The $I(J^P) = 1(1^+)$ A_1 is quite small (figures 19a,b) in the A_1 region ($1.06 \leq M_{3\pi} \leq 1.2$ GeV). For a width less than 150 MeV we estimate $\sigma(A_1) < 3.5\mu b$. An A_1 hiding under the A_2 as proposed in reference 28 is also excluded. The $1(2^-)$ A_3 (figures 20a,b) although large does not exhibit a resonance like structure. The peaks differ in the two t bins and also differ from that observed in the reactions $\pi^- p \to \pi^0\pi^+\pi^- p$[1,2,29,10]. The

$0(1^+)$ wave (figure 21) wave has a peak at the B meson mass, but has $\sigma < 4.5\ \mu b$ for a width of 150 MeV in this region and exists only at low t. However, it is comparable to the "A_1" in magnitude. The only other large background wave, the $1(0^-)$ is shown in figures 22a,b. The I=2 background, shared among many angular momentum states is shown in figures 23a,b.

There is also a low mass enhancement for the 1^+ I=0 waves which is partly due to misidentified photons from η' decays[31]. The production cross section for $\Delta^{++}\eta'$ production for this experiment[7] is $14.7 \pm 1.7\ \mu b$ when the Δ^{++} Breit-Wigner is integrated. 250 fake events coming from the decay $\eta' \to \pi^+\pi^-\gamma$ were generated and of these 209 fit the hypothesis $\pi^+\pi^-\pi^0$ [32]. This fact, together with the known branching ratio of .27[22] of η' into $\pi^+\pi^-\gamma$, gives approximately 90 events of η' contamination in the region $.9 \le M_{3\pi} \le 1.06$ GeV. C conservation and Bose statistics require that the $\pi^+\pi^-$ system have odd spin (henceforth, we assume spin one). Since the η' is spinless, there can be no preferred orientation in the decay into $\rho^0\gamma$. Therefore, when the photons are misidentified as pions, we expect the ρ"π" distribution to be S-wave. The I = 0,2 1^+S $\rho\pi$ amplitudes coming from the analysis are such that when $\rho\pi$ charge eigenstates are formed in the region $.82 \le M_{3\pi} \le 1.06$ GeV, we find 240 $\rho^0\pi^0$ events. This is more than we expected from η' contamination and accounts for most of the I = 0,2 signals. Furthermore, the Illinois group[33] has pointed out that the

smallness of the Dalitz plot in this region makes distinguishing 1^+P_f and 1^+S_p waves difficult. This is just another face of the problems caused when the unitarity violating isobar model is used to fit regions with large overlaps of resonance bands. Therefore, results for this low mass region for 1^+ waves should be viewed with some caution.

We now turn to a discussion of the t-dependence of the resonances. All of the quoted distributions, in what follows, have been corrected for t_{min} effects by scaling the observed number of events to equal phase space volumes. For the A_2 this is a factor of two correction in the lowest t-interval, while for the ω° this amounts to a tenfold increase. Figure 24 shows the A_2 differential cross sections together with the total differential cross section in that region, while figure 25 gives the natural and unnatural contributions to the A_2. Figure 26 shows the total ω° differential cross section and the total differential cross section for $1.6 \leq M_{3\pi} \leq 1.8$ GeV, while figure 27 gives the natural and unnatural contributions to the ω°. The ratio R of natural to unnatural exchange contributions calculated from these graphs is slightly different from that given previously. The previous numbers come from including all resonant events, and here we have taken only a 200 MeV wide slice in meson mass.

There is another prediction of semi-inclusive duality collateral to equation 28, namely

$$\frac{d\sigma_i}{dt}(m^2) \sim e^{-2\alpha_i' t \ln(m^2)} \qquad (29),$$

where i corresponds to either natural or unnatural exchange, α_i' is the slope of the Regge trajectory i, and m is the mass of the resonance. If we assume a slope of one for the trajectories, then this formula predicts that the slope of the t-distribution decrease by 2 and 3 units for A_2 and ω^*, respectively, relative to the ω. In figures 28 and 29 we plot the natural and unnatural exchange contributions to ω^{27}, A_2 and ω^* production. The lines are the results of fits of $A\, e^{bt}$ to the approximately exponential regions of the t-distributions. For natural exchange contributions we find: $b_\omega = 5.58 \pm .44$, $b_{A_2} = 4.42 \pm 1.04$, and $b_{\omega^*} = 6.2 \pm 4$. So within these large errors the results are consistent with the antishrinkage prediction. For unnatural exchange contributions we have $b_\omega = 3.43 \pm .39$, $b_{A_2} = 3.29 \pm .74$ and $b_{\omega^*} = 3.17 \pm .67$, in disagreement with theory.

The relative phase between the T_{11}^{1+} and T_{10}^{0-} A_2 amplitudes is $\approx$ 70° (figure 28b). We remind the reader that our unnatural exchange amplitudes differ by a minus sign from the usual convention. This implies that the π-ρ-A_2 and π-B-A_2 couplings are of opposite sign, if the phase between the amplitudes is to be compatible with that coming from the Regge signature factor $e^{-i\pi\alpha/2}$ and $.5 \leq \alpha_\rho - \alpha_B \leq 1$.

The relative phase between T_{10}^{0-} [$1(2^+)$] and the T_{20}^{0+} [$1(0^-)$] shows a 180° change around $t \sim -0.175$ (figure 28a). We see that

this is reflected in the $|T^{0-}_{10}|^2$ A_2 intensity which has a dip in the same region(figure 29a), as does the net helicity flip zero amplitude $1/2(T^{1+}_{11} - T^{1-}_{11})$ (figure 29b). This is behavior is characteristic of the Bessel function $J_0(b\sqrt{-t})$ suggested by various absorption models[34,35]. However, these absorption models specify their structure in the s-channel helicity frame (SCH). When we crossed our amplitudes to the SCH the previously observed structure becomes much less marked (figures 30a,b). Note, however, that an amplitude which is essentially helicity conserving in one coordinate system (as in this case) will lose successively larger amounts of cross section to other amplitudes in another coordinate system as the crossing angle increases. The effect of this is to wash out structure at low |t| with a general decrease in cross section at higher values of |t|: we replace one "lumpy" amplitude by many smooth ones. Furthermore, an effect concentrated in the region .15<|t|.2 is mainly frame independent since the crossing angle is small here.

VI. Conclusions

The first partial wave analysis of the reaction $\pi^+p \to \Delta^{++}(\pi^+\pi^-\pi^0)$ has been performed. In the $(3\pi)^0$ mass distribution between 0.82 and 1.9 GeV, we have observed the A_2 and a peak due to the production of a 3^- ω^* state with the same mass as the g meson. No

significant A_1 production has been found. Resonance production agrees with the predictions of the quark model and some of those of semi-inclusive duality. Evidence for possible absorptive effects in A_2 production was given. The background waves behave very similarly to the corresponding ones found in other 3π systems, although their production mechanism violates the additivity assumption of the quark model.

Finally, we mention some problems which remain for future investigaton. Better methods are required for comparing the fits with the data than those involving binning data. The effect of measurement errors and finite experimental resolution should be taken into account in the fits. More work must be done to understand the extent to which the isobar model violates the axioms of unitarity and analyticity of S-matrix theory. This is important for two reasons. First, our inferences regarding meson spectroscopy would be suspect if the model on which they are based were in violent disagreement with the accepted principles of physics. Second, developing reliable techniques for calculations in strong interactions is in itself a laudable goal and three meson physics seems an ideal testing ground for such methods.

In this analysis we found major contributions from S $\dot{T}$ vectors. We were able to distinguish these by using information from the decay of the Δ^{**}. However, this incoherence can arise not only from production dynamics (as we supposed), but also can

come from averaging over bins where there are rapid variations in productions matrix elements. That this is a major problem in this analysis is unlikely, since the structure of $\vec{T}$ vectors was unchanged when we changed from an energy independent parametrization of the resonances to an energy dependent one. Nevertheless, this will be checked when the large increase in statistics due to the large multiparticle spectrometers allows finer binning.

Repetition of this analysis on data at other energies seems quite worthwhile. It would not only check this analysis, but also offer new information about Regge phenomenology: we would have independent determinations of Regge trajectories from phase behavior and energy dependence. A study of the reaction $K^-p \to (3\pi)^0\Lambda^0$ could be accomplished with minor changes in technique. In this reaction the Λ^0 polarization can be directly measured so no assumptions concerning the spin structure at the baryon vertex need be made.

Acknowledgements

During my stay at Berkeley I have profited by my associations with many people--too many to hope that this final thanks can be complete. Some of these, however, deserve special mention. My collaborators, Ed Ronat, Tom Lasinski and Fritz Wagner have been sources of much instruction and enthusiasm. My fellow graduate students, Fred Buhl, Ron Longacre and Dave Neuffer have helped to keep the travail in proper perspective. My advisor, Art Rosenfeld, has been invariably helpful. Discussions with Phillipe Eberhard concerning statistics and fitting programs have been enlightening. Finally, my parents have provided the encouragement and upbringing which made this thesis possible.

This work was performed under the auspices of the United States Energy Research and Development Administration.

Appendix A:Meson Decay Amplitude

Before we begin a detailed description of the formalism we give a qualitative discussion of the problems faced in fitting 3-body final states and our motivations for adopting the isobar model.

There are 3N-4 independent kinematic variables, in this case 5 (in formation reactions one of these is trivial), required to describe an N particle final state. For this problem one possible choice is: one dipion invariant mass, one dipion decay angle and a set of 3 Euler angles which describe the orientation of the plane defined by the three pions with respect to some external coordinate system. This choice of variables is picked with a sequential decay picture in mind. Now we have some decay amplitude $f(m_{\pi\pi};\theta_D;\alpha,\beta,\gamma)$ which, when squared, gives the distribution of the outgoing pions. If $G_i(\theta_D)$ and $H_j(\alpha,\beta,\gamma)$ are complete sets of orthogonal functions,

$$f = \sum_{i,j} a_{i,j}(m_{\pi\pi})\, G_i(\theta_D)\, H_j(\alpha,\beta,\gamma) \qquad (A.1).$$

There are certain practical problems with the expansion given for f. It is not manifestly Bose symmetric. Thus, any biases introduced in data reduction are propagated to the expansion parameters, $a_{ij}(m_{\pi\pi})$, which therefore have no simple physical interpretation. This can be remedied by writing the amplitude in the following symmetrized form:

$$f = \sum_{k=1}^{3} \sum_{i,j=1}^{\infty} a_{ij}^{k}(m_{\pi\pi}^{k})\, G_i(\theta_D^k)\, H_j(\alpha^k,\beta^k,\gamma^k) \qquad (A.2).$$

The label **k** indicates the choice of diparticle. The various symmetry properties amount to constraints on the $a_{ij}^{k}(m_{\pi\pi}^{k})$. Now we are left with the problem of determining the $a_{ij}(m_{\pi\pi})$ with limited statistics: 500–1000 events in a typical bin of 3 pion mass and momentum transferred squared. If one is interested only in the angular momentum properties of the initial state defined by the 3 Euler angles, one can bin in the remaining variables $m_{\pi\pi}$ and θ_D, or more symmetrically in the Dalitz plot variables, $s_{\pi\pi}^{(1)}$ and $s_{\pi\pi}^{(2)}$, and perform a moments analysis. Unfortunately, for a grid system as coarse as 5×5 this procedure gives us only 20 to 40 events per bin. Consequently, this will not become a viable procedure until statistics have improved by factors of 10–100. Therefore, to avoid binning on the Dalitz plot, a prescripton for the $s_{\pi\pi}$ dependence of the amplitude is required.

The isobar model supplies this prescription. It amounts to taking the sequential decay picture literally, that is, as a dynamical model not just an accounting device. It is motivated by the fact that resonance bands dominate the Dalitz plot.

The formalism now begins with some definitions of state vectors and their normalizations. If $\psi_{p\lambda}$ is a state of momentum p along the z-axis with helicity λ, the general state is then

$$|\vec{p}\,\lambda\rangle \equiv |p\ \theta\ \phi\ \lambda\rangle \equiv R(\phi,\theta,-\phi)\,\psi_{p\lambda} \qquad (A.3),$$

where R is the rotation operator. Our normalization is:

$$\langle \vec{p}' \lambda' | \vec{p} \lambda \rangle = 2E \, \delta^3(\vec{p}' - \vec{p}) \, \delta_{\lambda\lambda'} \qquad \text{(A.4)}.$$

Following Jacob and Wick[36] we define a χ state as:

$$\chi_{p\lambda} \equiv (-1)^{s-\lambda} R(0,\pi,0) \, \psi_{p\lambda} = (-1)^{s-\lambda} \psi_{-p,\lambda} \qquad \text{(A.5)},$$

where **s** is the intrinsic spin of the state. Multiparticle states are a direct product of single particle states:

$$|\vec{p}_1 \lambda_1, \vec{p}_2 \lambda_2, \cdots \vec{p}_n \lambda_n\rangle \equiv \prod_{i=1}^{n} |\vec{p}_i \lambda_i\rangle \qquad \text{(A.6)}.$$

For two particle states we introduce relative coordinates:

$$\vec{P} = \vec{p}_1 + \vec{p}_2 \, , \; \vec{p} = \frac{1}{2}(\vec{p}_1 - \vec{p}_2) \qquad \text{(A.7)},$$

and

$$|\vec{P},\vec{p},\lambda_1,\lambda_2\rangle = |\vec{p}_1,\lambda_1\rangle|\vec{p}_2,\lambda_2\rangle \qquad \text{(A.8)}.$$

To discuss the decomposition of two particle states into angular momentum states, it is convenient to work in the two particle center of mass and to take particle two as a χ-state. Thus,

$$|\vec{P} = 0,\vec{p},\lambda_1,\lambda_2\rangle = R(\phi,\theta,-\phi) \, \psi_{p,\lambda_1} \chi_{p,\lambda_2} \qquad \text{(A.9)}.$$

The angular momentum states are then defined by:

$$|\vec{P} = 0,p,J,M,\lambda_1,\lambda_2\rangle = N_J \int D^{J*}_{M\lambda}(\phi,\theta,-\phi) \, |\vec{P} = 0,\vec{p},\lambda_1,\lambda_2\rangle \, d\Omega \, \text{(A.10)}.$$

Here, J is the total angular momentum, M is it z-component, $\lambda = \lambda_1 - \lambda_2$, and N_J, a normalization factor, is given by $\left(\frac{2J+1}{4\pi}\right)^{1/2}$ $\left(\frac{p}{4W}\right)^{1/2}$. W is the total energy in the center of mass. To convert from a helicity basis to an L-S basis we have the following formula:

$$|\vec{P} = 0,pJM,LS\rangle = \sum_{\lambda_1,\lambda_2} \left(\frac{2L+1}{2J+1}\right)^{1/2} \langle S_1 \lambda_1 S_2 -\lambda_2 | S \lambda_1 - \lambda_2\rangle \times \langle L \, 0 \, S \, \lambda_1 - \lambda_2 | J \, M\rangle \, |\vec{P} = 0,pJM,\lambda_1 \lambda_2\rangle \qquad \text{(A.11)}$$

Having disposed of preliminaries we now begin calculation of

the isobar amplitude , G. Consider an initial state $|n\ M\rangle_{S'}$, where M is the spin projection in an external coordinate system S' and n labels the set of quantum numbers $\{J, P, I, I_z\}$. However, we want to evaluate the decay amplitude in a body fixed coordinate system S:

$$G = {}_{S'}\langle \vec{Q}_j, \vec{Q}_k, \vec{Q}_l | T | n\ M\rangle_{S'} \qquad (A.12).$$

Here $\vec{Q}_j$, $\vec{Q}_k$, $\vec{Q}_l$ are the momenta in the three pion rest frame of the outgoing pions. $\{ j, k, l\}$ is a cyclic permutation of $\{1, 2, 3\}$, the latter set being a specific ordering of particles--say that on the data tape. But,

$${}_{S'}\langle \vec{Q}_j, \vec{Q}_k, \vec{Q}_l | T | n\ M\rangle_{S'} = \sum_m {}_S\langle \vec{Q}_j, \vec{Q}_k, \vec{Q}_l | T | n\ M\rangle_S\ D^J_{mM}(\alpha,\beta,\gamma)$$

(A.13).

With $(\hat{x}, \hat{y}, \hat{z})$ and $(\hat{x}', \hat{y}', \hat{z}')$ the basis vectors in systems S and S', respectively, the Euler angles are given by:

$$\alpha = \tan^{-1}\left(\frac{\hat{z}'\cdot\hat{y}}{\hat{z}'\cdot\hat{x}}\right) \qquad (A.14)$$

$$\beta = \cos^{-1}(\hat{z}\cdot\hat{z}') \qquad (A.15)$$

$$\gamma = \tan^{-1}\left(\frac{\hat{x}'\cdot\hat{z}}{\hat{y}'\cdot\hat{z}}\right) \qquad (A.16)$$

Introducing a sequential decay scheme, $T = T_2T_1$, we have

$$\langle \vec{Q}_j, \vec{Q}_k, \vec{Q}_l | T | n\ m\rangle = \sum_{\mu_n} \int \frac{d^3Q_m}{2E_m}\frac{d^3Q_n}{2E_n}\ 2E_n\ \delta^3(\vec{Q}_m + \vec{Q}_n)$$
$$\langle \vec{Q}_j, \vec{Q}_k, \vec{Q}_l | T_2 | \vec{Q}_n, \mu_n; \vec{Q}_m\rangle\langle \vec{Q}_n,\mu_n ; \vec{Q}_m | T_1 | n\ m\rangle$$

(A.17)

We have just assumed that only two particle intermediate states

contribute. We now make one further assumption: T_2 acts only on $|\vec{Q}_n, \mu_n\rangle$. Therefore,

$$\langle \vec{Q}_j, \vec{Q}_k, \vec{Q}_l | T_2 | \vec{Q}_n \mu_n ; \vec{Q}_m \rangle = 2E_m \delta^3(\vec{Q}_j - \vec{Q}_m)\langle \vec{Q}_k, \vec{Q}_l | T_2 | \vec{Q}_n \mu_n \rangle$$

(A.18).

Consequently,

$$\langle \vec{Q}_j, \vec{Q}_k, \vec{Q}_l | T | n\ m \rangle = \sum_{\lambda_j} \langle \vec{Q}_k, \vec{Q}_l | T_2 | -\vec{Q}_j\ j \rangle \langle \vec{Q}_j, -\vec{Q}_j\ \lambda_j | T_1 | n\ m \rangle \quad \text{(A.19)}.$$

Here the isobar is taken to be a χ state with helicity λ_j. Decomposing $\langle \vec{Q}_j, -\vec{Q}_j\ \lambda_j |$ into angular momentum states we have,

$$\langle \vec{Q}_j, -\vec{Q}_j\ \lambda_j | T_1 | n\ m \rangle = \left(\frac{2J+1}{4\pi}\right)^{1/2} \left(\frac{4W}{Q_j}\right)^{1/2} D^{J*}_{m,-\lambda_j}(\Omega) \times \langle Q_j\ Jm, \lambda_j | T_1 | J\ n\ m \rangle \quad \text{(A.20)}.$$

If we choose the $\hat{z}$ axis of the system S along $\vec{Q}_j$ and the $\hat{y}$ axis normal to the 3-pion plane, the argument of the rotation function vanishes and the function becomes a Kronecker delta in its indices. Thus,

$$\langle \vec{Q}_j, -\vec{Q}_j\ \lambda_j | T_1 | n\ m \rangle = \delta_{m,-\lambda_j} \left(\frac{2J+1}{4\pi}\right)^{1/2} \left(\frac{4W}{Q_j}\right)^{1/2} \langle Q_j, Jm, \lambda_j | T_1 | Jnm \rangle$$

(A.21).

To fix the parity of the system it is convenient to convert from helicity to LS states. Using (A.11) we have:

$$|Q_j, Jm, \lambda_j\rangle = \sum_{L_j S_j} \left(\frac{2L_j+1}{2J+1}\right)^{1/2} \langle L_j\ 0\ S_j\ -\lambda_j | J\ m \rangle\ |J\ L_j\ S_j\ m\rangle$$

(A.22).

S_j, L_j are the spin of the isobar and the relative orbital angular momentum between the isobar and the odd pion, respectively, and

$(j_1\ m_1\ j_2\ m_2|\ J\ M)$ is a Clebsch-Gordan symbol. Thus,

$$\langle \vec{Q}_j; -\vec{Q}_j\ \lambda_j|\ T_1\ |\ n\ m\rangle = \sum_{L_jS_j} \delta_{m,-\lambda_j} \left(\frac{2L_j+1}{\pi}\right)^{1/2} \left(\frac{W}{Q_j}\right)^{1/2} (L_j\ 0\ S_j\ -\lambda_j|J\ m)\langle J\ L_j\ S_j\ m|\ T_1\ |J\ m\ n\rangle \tag{A.23}$$

Using rotational invariance we write

$$\langle J\ L_j\ S_j\ m|\ T_1\ |\ J\ m\ n\rangle = T^{Jn}_{L_jS_j}(W,\ t,\ w_j) \tag{A.24}$$

where w_j is the mass of the diparticle. We now evaluate the T_2 matrix element in the rest frame of the isobar.

$$\langle \vec{Q}_k,\vec{Q}_l|\ T_2\ |\ -\vec{Q}_j,\lambda_j\rangle = \langle \vec{q}_k,\vec{q}_l|\ T_2\ |S_j,-\lambda_j\rangle \tag{A.25}$$

$\vec{q}_k$ is the momentum of pion k in the dipion rest frame. Performing an angular momentum decomposition, we have

$$\langle \vec{Q}_k,\vec{Q}_l|\ T_2\ |\ -\vec{Q}_j,\lambda_j\rangle = \left(\frac{w_j}{\pi q_k}\right)^{1/2} (2S_j+1)^{1/2}\ D^{S_j*}_{-\lambda_j,0}(\text{decay}) \times \langle q_k\ S_j\ -\lambda_j|\ T_2\ |S_j\ -\lambda_j\rangle \tag{A.26}$$

By rotational invariance, the last factor may be written as $B^{S_j}(w_j)$. We are free to pick a coordinate system such that

$$D^{S_j*}_{-\lambda_j,0}(\text{decay}) = d^{S_j}_{\lambda_j,0}(\theta_D) \tag{A.27}$$

Finally, we can write

$$_S\langle \vec{Q}_j\ \vec{Q}_k\ \vec{Q}_l|\ T\ |nM\rangle_S = \sum_n \kappa_n(j)\ T_n(W,\ w_j,\ t) \tag{A.28}$$

where

$$T_n(W,w_j,t) = T^{Jn}_{L_jS_j}(W,w_j,t)\ B^{S_j}(w_j) \tag{A.29}$$

and

$$\kappa_n(j) = \frac{1}{\pi}\left(\frac{Ww_j}{q_kQ_j}\right)^{1/2} (2L_j+1)^{1/2}(2S_j+1)^{1/2} \sum_{\lambda_j} d^{S_j}_{\lambda_j,0}(\theta_D)\ D^{J}_{-\lambda_jM}(\alpha,\beta,\gamma)$$

$$(L_i\ 0\ S_i\ -\lambda_i|j\ -\lambda_i)$$

(A.30).

Near threshold $T^{Jn}_{L_i>_i}(W,w_i,t)$ should be governed by barrier penetration factors. In our normalization we take these to equal

$$\left(\frac{Q}{W}\right)^{1/2}|(Q_iR)\,|h^{(1)}_{L_i}(Q_iR)|^{-1} \qquad \text{(A.31)},$$

where R is a radius of interaction, taken in this analysis to be one fermi, and $h^{(1)}_{L_i}(x)$ is the spherical Hankel function of the first kind of order L_i. The charge dependence can also be made explicit by using isospin Clebsch-Gordan symbols. Therefore,

$$T^{Jn}_{L_i>_i}(W,w_i,t) = \left(\frac{Q}{W}\right)^{1/2}|t^{Jn}_{L_i>_i}(W,w_i,t)\,|(Q_iR)\,|h^{(1)}_{L_i}(Q_iR)|^{-1}$$
$$\times (I^{\pi\pi}\ I^{\pi\pi}_z\ 1\ I^{\pi}_z|I\ 0) \qquad \text{(A.32)}$$

for a neutral three pion system. Similarly, the charge dependence can be removed from $B^{>}_{\lambda}(w_i)$:

$$B^{>}_{\lambda}(w_i) = (1\ I^{\pi}_z\ 1\ I^{\pi}_z|I\ I^{\pi\pi}_z)\,A^{>}_{\lambda}(w_i) \qquad \text{(A.33)}.$$

$A^{>}_{\lambda}(w_i)$ is given by the Watson theorem[17].

$$A^{>}_{\lambda} = (e^{i\delta}\sin\delta)/q^{>}_{k}{}^{l+1} \times (w_i q_k)^{1/2} \qquad \text{(A.34)}$$

δ is the elastic scattering phase shift at the mass w_i. A factor $(q_k)^{1/2}$ is added to insure proper threshold behavior in this normalization.

The following forms were used for the phase shifts. For the I = 0 S-wave, ϵ, we used the phase shifts of the CERN-Munich spectrometer group[18] with their energy dependent parameterization:

$$e^{i\delta}\sin\delta = \frac{k_{\pi\pi}q_\pi - i\,\det|K|q_\pi q_K}{1 - \det|K|q_\pi q_K - i(k_{\pi\pi}q_\pi + k_{KK}q_K)} \qquad \text{(A.35)},$$

where $q_\pi(q_K)$ is the momentum of the pion(kaon) in a dipion(dikaon) system of energy w. The symmetric K-matrix is given by:

$$K_{ij} = \frac{\alpha_i\alpha_j}{s_1 - w^2} + \frac{\beta_i\beta_j}{s_2 - w_2} + \gamma_{ij} \qquad \text{(A.36)}.$$

The parameters in appropriate powers of GeV are: $\sqrt{s_1} = .11$, $\sqrt{s_2} = 1.19$, $\gamma_{\pi\pi} = 2.86$, $\alpha_\pi = 2.28$, $\beta_\pi = -1.00$, $\gamma_{\pi K} = 1.85$, $\alpha_K = 2.02$, $\beta_K = .47$, $\gamma_{KK} = 1.00$. The I = 1 P-wave, ρ, phases are given by the parametrization of Morgan[39]:

$$\cot\delta = (m_\pi^2 - 0.1536q^2)(m_\pi^2 + 0.028q^2)(m_\pi^2 + q^2)^{1/2}/(0.035m_\pi^2 q^4) \qquad \text{(A.37)}.$$

The I = 0 D-wave, f, is given by a relativistic Breit-Wigner formula:

$$\cot\delta = \frac{(1.264)^2 - w^2}{1.264\Gamma} \qquad \text{(A.38)},$$

and

$$\Gamma = .150\frac{(q_0R)^2|h_2^{(1)}(q_0R)|^2}{(qR)^2|h_2^{(1)}(qR)|^2} \qquad \text{(A.39)},$$

where R is one fermi and q_0 is a pion momentum at resonance.

We must deal with isobars in other diparticle combinations as well. While an expansion in one type of isobar is complete, the description of resonances in other diparticle combinations would require prohibitively many terms. Therefore, we write our amplitude as a coherent sum over different diparticle combinations. This procedure while justified in the limit of infinitely narrow isobars, violates unitarity when resonance bands overlap on the Dalitz plot. Two groups[40,41] have studied this problem and produced "unitarized" amplitudes which were then fit

to the data. Both groups use a K-matrix technique with purely on-shell amplitudes and arrive at the same Volterra equation from somewhat different starting points. They find that these new amplitudes, when fit to the data, produce results not qualitatively different from the old but with appreciably worse likelihoods. Aitchinson[42] argues that the cause of this failure is the mass shell condition of the K-matrix formalism. That is, in the process of removing cuts due to normal thresholds in the subenergies, extra subenergy dependence has been introduced into the amplitude. This is a disaster since the isobar model is used mainly because its fitting parameters have,hopefully, minimal subenergy dependence. Consequently, although there is continuing work on this problem, the conventional isobar prescription seems the best currently available.

If we assume that the only diparticle mass dependence is that given explicitly, and place all factors depending only on W and t in the production matrix element for the overall reaction, we obtain the amplitude for decay via a particular isobar (notice that the set, n, of quantum numbers has been expanded to include isobar labels):

$$G^{J^P M}_{[SLI_{iso}]}(W,t) = (2L+1)^{1/2}(2S+1)^{1/2}\sum_j \{\langle I^{iso}\ I_z^{iso}\ 1\ I_z^j | I\ 0\rangle \langle 1\ I_z^k\ 1\ I_z^j | I^{iso}\ I_z^{iso}\rangle (Q_jR)^{-1} |h_L^{(1)}(Q_jR)|^{-1} \frac{e^{i\delta}\sin\delta}{q_k^{S+1}} w_j \sum_\lambda d^S_{-\lambda,0}(\theta_b^j)\, D^J_{-\lambda,M}(\alpha^j,\beta^j,\gamma^j) \langle L\ 0\ S\ -\lambda | J\ -\lambda\rangle \}$$

(A.40).

Notice that there is a different set of angles for each dipion combination. θ_D^j is the angle, in the dipion rest frame, between particle j (the odd pion) and particle k. The normal to the three pion plane, the Y axis of system S, is defined by $\vec{Q}_j \times \vec{Q}_k$.

To check that our amplitude obeys Bose statistics, we see what changes occur when particles k and l are interchanged. The following changes occur in the arguments of the functions:

$$\theta_D^j \to \pi - \theta_D^j, \quad \theta_D^k \to \pi - \theta_D^l, \quad \theta_D^l \to \pi - \theta_D^k;$$

$$w_j \to w_j, \quad w_k \to w_l, \quad w_l \to w_k;$$

$$Q_j \to Q_j, \quad Q_k \to Q_l, \quad Q_l \to Q_k;$$

$\vec{Y} \to -\vec{Y}$ implies

$$\alpha_j \to \alpha_j + \pi, \quad \alpha_k \to \alpha_l + \pi, \quad \alpha_l \to \alpha_k + \pi;$$

$$\beta_j \to \beta_j, \quad \beta_k \to \beta_l, \quad \beta_l \to \beta_k;$$

$$\gamma_j \to \gamma_j, \quad \gamma_k \to \gamma_l, \quad \gamma_l \to \gamma_k;$$

and for the isospin labels

$$I_z^j \to I_z^j, \quad I_z^k \to I_z^l, \quad I_z^l \to I_z^k \qquad \text{(A.41).}$$

These changes have the following effects on the components of G.

1) If particle j is the odd particle(not in the dipion combination):

$$D^J_{-A,M}(\alpha^j,\beta^j,\gamma^j) \to (-1)^A D^J_{-A,M}(\alpha^j,\beta^j,\gamma^j)$$

$$d^S_{-A,0}(\theta_D^j) \to (-1)^{S-A} d^S_{-A,0}(\theta_D^j)$$

$$(1\ I_z^k\ 1\ I_z^l |\ I^{iso}\ I_z^{iso}) \to (-1)^{I_{iso}} (1\ I_z^k\ 1\ I_z^l |\ I^{iso}\ I_z^{iso}) \qquad \text{(A.42).}$$

If $(-1)^{I_{iso}+S} = 1$, the contribution to G from j-type isobars is invariant under interchange of the particles composing it. This

condition is just that imposed by generalized Bose statistics.

2) If particle k was originally the odd particle(the one not in the isobar), under k−l interchange we obtain:

$$D^J_{-\Lambda,M}(\alpha^k,\beta^k,\gamma^k) \to (-1)^\Lambda D^J_{-\Lambda,M}(\alpha^l,\beta^l,\gamma^l)$$

$$d^S_{-\Lambda,0}(\theta^k_D) \to (-1)^{S-\Lambda} d^S_{-\Lambda,0}(\theta^l_D)$$

$$\langle I^{iso} I^z_{iso} 1 I^k_z | I 0\rangle \to \langle I^{iso} I^z_{iso} 1 I^l_z | I 0\rangle$$

$$\langle 1 I^l_z 1 I^j_z | I^{iso} I^{iso}_z\rangle \to (-1)^{I_{iso}} \langle 1 I^j_z 1 I^k_z | I^{iso} I^{iso}_z\rangle \qquad (A.43).$$

This just interchanges the contributions of k and l type isobars. Therefore, G satisfies generalized Bose statistics.

The function g obeys a symmetry under the interchange M → −M. Consider the factor of g for dipion j,

$$\sum_\Lambda d^S_{-\Lambda,0}(\theta^j_D) D^J_{-\Lambda,M}(\alpha^j,\beta^j,\gamma^j) \langle L\ 0\ S\ -\Lambda | J\ -\Lambda\rangle \qquad (A.44),$$

all other factors being invariant under this interchange. From this select the partial sum

$$K(M) = d^S_{-\Lambda,0} D^J_{-\Lambda,M} \langle L\ 0\ S\ -\Lambda | J\ -\Lambda\rangle + d^S_{\Lambda,0} D^J_{\Lambda,M} \langle L\ 0\ S\ \Lambda | J\ \Lambda\rangle$$

(A.45).

Using well known properties of Clebsch−Gordan coefficients and rotation functions, we obtain

$$K = (D^J_{-\Lambda,M} + (-1)^{L+S-J-M} D^{J*}_{-\Lambda,-M}) \langle L\ 0\ S\ -\Lambda | J\ -\Lambda\rangle d^S_{-\Lambda,0} \qquad (A.46).$$

Apparently,

$$K(-M) = (-1)^{L+S-J-M} K^*(M) \qquad (A.47).$$

Since the whole function g(M) is obtained from linear combinations of the K(M)'s, we have:

$$g(-M) = (-1)^{L+S-J-M} g^*(M) \qquad (A.48).$$

Consequently, the linear combinations of G's, which multiply the parity conserving amplitudes, are composed of terms proportional to Re(g) for $\eta = +1$, and Im(g) for $\eta = -1$.

Appendix B: The Spin Averaged Intensity

In this section we calculate the spin averaged intensity. We consider not only $J^P = \frac{3}{2}^+$ πp systems, but also $J^P = \frac{1}{2}^-$, S-wave systems for which $Y_B = -1$. If we abbreviate $(\vec{T}\cdot\vec{G})^{\eta}_{S,|\mu|}$ by $T^{\eta}_{S,|\mu|}$, we can write

$$T_{\lambda_p,\lambda_{p'}} = \sum_{S,|\mu|,\eta} T^{\eta}_{S,|\mu|} H^{\eta}_{S,|\mu|} \tag{B.1},$$

where

$$H^{\eta}_{S,|\mu|} = \sum_{a} x_a^{S|\mu|\eta} H_{S,a} \tag{B.2},$$

and

$$x_a^{S|\mu|+} = \frac{\gamma(a)}{2\epsilon(a)}\left[\delta_{a,-|\mu|} + Y_B\delta_{a,|\mu|}\right] \tag{B.3},$$

and

$$x_a^{S|\mu|-} = \frac{i\gamma(a)}{2\epsilon(a)}\left[\delta_{a,-|\mu|} - Y_B\delta_{a,|\mu|}\right] \tag{B.4}.$$

Substituting for $H_{S,a}$, we have

$$T_{\lambda_p,\lambda_{p'}} T^{*}_{\lambda_p,\lambda_{p'}} = \sum_{\substack{S,|\mu|,\eta \\ S',|\mu'|,\eta' \\ a,a' \\ \lambda_\Delta,\lambda_{\Delta'}}} T^{\eta}_{S,|\mu|}\, T^{\eta'*}_{S',|\mu'|}\, \frac{1}{2}\sqrt{2S+1}\sqrt{2S'+1}\, \langle\tfrac{1}{2}\lambda_p\, S\, a|\, J\, \lambda_\Delta\rangle\, D^{J*}_{\lambda_\Delta,\lambda_p}\, \langle\tfrac{1}{2}\lambda_p\, S'\, a'|\, J'\, \lambda_{\Delta'}\rangle\, D^{J'}_{\lambda_{\Delta'},\lambda_{p'}}\, x_a^{S|\mu|\eta}\, x_{a'}^{S'|\mu'|\eta'*} \tag{B.5}.$$

Now,

$$D^{J*}_{\lambda_\Delta,\lambda_p}\, D^{J'}_{\lambda_{\Delta'},\lambda_{p'}} = (-1)^{\lambda_\Delta-\lambda_{p'}} \sum_{L} \langle J\, -\lambda_\Delta\, J'\, \lambda_{\Delta'}|\, L\, M\rangle\, D^{L}_{M,0}\, \langle J\, -\lambda_{p'}\, J'\, \lambda_{p'}|\, L\, 0\rangle \tag{B.6}.$$

Therefore, summing over the outgoing proton helicity ($\lambda_{p'}$), we obtain:

$$\Sigma\,(-1)^{\lambda_{p'}}(J\ -\lambda_{p'}\ J'\ \lambda_{p'}|\ L\ 0) = \delta_{L,1}(-1)^{1/2}\sqrt{2}(\delta_{J,3/2}\delta_{J',1/2} + \delta_{J,1/2}\delta_{J',3/2})$$

$$+\ \delta_{L,0}(-1)^{1/2}\sqrt{2}(\delta_{J,1/2}\delta_{J',1/2})$$

$$+\ (-1)^{(L+3)/2}\ \delta_{J,3/2}\ \delta_{J',3/2}(\delta_{L,0} + \delta_{L,2})$$

(B.7).

If we write,

$$Y(S,S',\eta,\eta',|\mu|,|\mu'|,\alpha,\alpha',J,J',L)$$

$$= \frac{1}{4}T^{\eta}_{S,|\mu|}\,T^{\eta'*}_{S',|\mu'|}\,\chi^{S,|\mu|,\eta}_{\alpha}\,\chi^{S',|\mu'|,\eta'*}_{\alpha'}\sqrt{2S+1}\ \sqrt{2S'+1}$$

(B.8),

then the spin averaged intensity equals

$$\sum_{\substack{S,S',\eta,\eta',|\mu|,|\mu'|\\ \alpha,\alpha',J,J',L}} Y \times (\Sigma\,(-1)^{\lambda_{p'}}(J\ -\lambda_{p'}\ J'\ \lambda_{p'}|\ L\ 0))$$

$$\times\ \sqrt{2L+1}\ \sqrt{2J+1}\ \sqrt{2J'+1}(-1)^{J'-J+S+S'-1}$$

$$\times\sum_{\lambda_{\Delta},\lambda_{p},\lambda_{\Delta'}} (-1)^{-\lambda_{\Delta'}-M}\begin{pmatrix} J & J' & L\\ -\lambda_{\Delta} & \lambda_{\Delta'} & -M\end{pmatrix} D^{L}_{M0}$$

$$\begin{pmatrix} 1/2 & S & J\\ \lambda_{p} & \alpha & -\lambda_{\Delta}\end{pmatrix}\begin{pmatrix} 1/2 & S' & J'\\ \lambda_{p} & \alpha' & -\lambda_{\Delta'}\end{pmatrix} \qquad (B.9),$$

where $\begin{pmatrix} j_1 & j_2 & J\\ m_1 & m_2 & -M\end{pmatrix}$ is a Wigner 3j symbol. The inner sum equals,

$$(-1)^{1/2+\alpha'+S'+S+L}\begin{pmatrix} S' & L & S\\ -\alpha' & M & \alpha\end{pmatrix}\begin{Bmatrix} S' & L & S\\ J & 1/2 & J'\end{Bmatrix} \qquad (B.10),$$

where the braces denote a Wigner 6j symbol. Substituting (B.7), (B.8), and (B.10) into (B.9) and performing some tedious arithmetic we find the following expression for the spin averaged intensity, I:

$$8\pi\ I = \Sigma\ X_i\ A_{in}\ X^{*}_{n} \qquad (B.11),$$

where $\vec{X}$ is the n-tuple $(T^{+}_{1,1},T^{-}_{1,0},T^{-}_{1,1},T^{-}_{0,0},T^{-}_{2,1},T^{+}_{2,0},T^{+}_{2,1})$, and in terms of the components of a unit vector, $\hat{p}'$, along the direction of the outgoing proton in the delta rest frame, the symmetric matrix

A is:

$$
\begin{array}{ccccccc}
\frac{3}{2}p_y^2+\frac{1}{2} & \frac{3}{2}p_yp_z & -\frac{3}{2}p_yp_x & \sqrt{2}p_y & \frac{\sqrt{3}}{2}p_yp_x & -\frac{\sqrt{3}}{2}p_yp_z & \\
\frac{3}{2}p_yp_z & \frac{3}{2}p_z^2+\frac{1}{2} & -\frac{3}{2}p_zp_x & \sqrt{2}p_z & -\frac{\sqrt{3}}{2}p_zp_x & 0 & \frac{\sqrt{3}}{2}p_zp_y \\
\frac{3}{2}p_zp_x & \frac{3}{2}(p_x^2-p_z^2) & & & & & \\
-\frac{3}{2}p_yp_x & -\frac{3}{2}p_zp_x & \frac{3}{2}p_x^2+\frac{1}{2} & -\sqrt{2}p_x & \frac{\sqrt{3}}{2}(p_y^2-p_z^2) & & \frac{3}{2}p_zp_y \\
\sqrt{2}p_y & \sqrt{2}p_z & -\sqrt{2}p_x & 1 & 0 & 0 & 0 \\
\frac{\sqrt{3}}{2}p_yp_x & & & & & & \\
\frac{\sqrt{3}}{2}p_yp_x & -\frac{\sqrt{3}}{2}p_zp_x & \frac{\sqrt{3}}{2}(p_y^2-p_z^2) & & 0 & \frac{3}{2}(1-p_x^2) & -\frac{\sqrt{3}}{2}p_yp_z \\
\frac{3}{2}p_zp_x & 0 & -\frac{3}{2}p_zp_y & 0 & -\frac{\sqrt{3}}{2}p_zp_y & \frac{3}{2}p_z^2+\frac{1}{2} & -\frac{\sqrt{3}}{2}p_zp_x \\
\frac{\sqrt{3}}{2}(p_x^2-p_z^2) & & \frac{\sqrt{3}}{2}p_zp_y & \frac{\sqrt{3}}{2}p_yp_x & 0 & \frac{3}{2}p_yp_x & -\frac{\sqrt{3}}{2}p_zp_x \\
\frac{3}{2}(1-p_y^2) & & & & & & (B.12).
\end{array}
$$

Table I

3π partial waves allowed in this analysis. The columns headed Iso contain the isobar: ϵ,ρ,or f. I is the total isospin. L is the orbital angular momentum between the isobar and the odd pion. J and P are the total angular momentum and the parity, respectively.

$.82 \le M_{3\pi} \le 1.2$ GeV					$1.2 \le M_{3\pi} \le 1.4$ GeV					$1.4 \le M_{3\pi} \le 1.9$ GeV				
Iso	I	L	J	P	Iso	I	L	J	P	Iso	I	L	J	P
ρ	0	0	1	+	ρ	0	1	0	−	ρ	0	0	1	+
ρ	0	1	2	−	ρ	0	0	1	+	ρ	0	1	2	−
ρ	0	1	0	−	ρ	0	1	2	−	ρ	0	2	3	+
ϵ	1	0	0	−	ϵ	1	0	0	−	ρ	0	2	1	+
ϵ	1	1	1	+	ϵ	1	1	1	+	ρ	0	1	0	−
ϵ	1	2	2	−	ϵ	1	2	2	−	ϵ	1	0	0	−
f	1	0	2	−	f	1	0	2	−	ϵ	1	1	1	+
ρ	2	0	1	+	ϵ	1	3	3	+	ϵ	1	2	2	−
ρ	2	1	2	−	f	1	1	1	+	f	1	0	2	−
ρ	2	1	0	−	f	1	1	3	+	ϵ	1	3	3	+
ρ	1	1	0	−	ρ	2	1	0	−	f	1	1	1	+
ρ	1	0	1	+	ρ	2	0	1	+	f	1	1	3	+
ρ	1	1	2	−	ρ	2	1	2	−	ρ	2	0	1	+
ρ	0	1	1	−	ρ	1	1	0	−	ρ	2	1	2	−
ρ	2	1	1	−	ρ	1	0	1	+	ρ	2	2	3	+
ρ	1	2	2	+	ρ	1	1	2	−	ρ	2	2	1	+
ρ	1	1	1	−	ρ	0	2	2	+	ρ	2	1	0	−
					ρ	0	1	1	−	ρ	1	1	0	−
					f	1	1	2	+	ρ	1	0	1	+
					ρ	2	2	2	+	ρ	1	1	2	−
					ρ	2	1	1	−	ρ	1	2	1	+
					ρ	1	2	2	+	ρ	1	2	3	+
					ρ	1	1	1	−	ρ	0	1	1	−
										ρ	0	3	3	−
										f	1	1	2	+
										ρ	2	1	1	−
										ρ	2	3	3	−
										ρ	1	2	2	+
										ρ	1	1	1	−

References and Footnotes

1. M. Tabak, E.E. Ronat, A.H. Rosenfeld, T.A. Lasinski, and R.J. Cashmore, Proceedings of the 4th International Conference on Experimental Meson Spectroscopy,Boston(1974) APS No.21 p.46 and Lawrence Berkeley Laboratory Report LBL-3010(May 1974).

2. Yu.M. Antipov, G. Ascoli, R. Busselo, M.N. Foccaci, W. Kienzle, R. Klanner, A. Lebedev, P. LeConte, V. Roinishvili, A. Weitsch, and F.A. Yotch, Nucl. Phys. B63(1973)153 and references therein.

3. G.L. Kane, to appear in the Proceedings of the 10th Annual Rencontre de Moriond, Meribel-les-Allues, March 1975.

4. E.L. Berger, Invited Paper Prepared for the Daresbury Meeting on Three-Particle Phase Shift Analysis and Meson Resonance Production, and Argonne Preprint ANL-HEP-PR-06(February 1975).

5. R.L. Ott(Ph.D. Thesis), Lawrence Berkeley Laboratory Report LBL-1547(1972).

6. S. Flatte', Lawrence Berkeley Laboratory Group A Physics Memo 646,1968(unpublished).

7. W.F. Buhl(Ph.D. Thesis), Lawrence Berkeley Laboratory Report LBL-4214(1975).

8. Many of the remaining peaks are not consistent with the position of known N*'s.

9. C.F. Cho and J.J. Sakurai, Physics Letters 30B(1969)119.

10. F. Wagner, Lawrence Berkeley Laboratory Report LBL-3611, in preparation.

22. Particle Data Group, Phys.Lett. 50B (1974)91.

23. G.C. Fox and A.J.G. Hey, Nucl.Phys.B65 (1973) 386.

24. M.J. Emms, G.T. Jones, J.B. Kinson, B.J. Stacey, M.F. Votruba, P.L. Woodworth, I.G. Bell, M. Dale, D. Evans, J.V. Major, J.A. Charlesworth, D.J. Crennel and R.L. Sekulin, Rutherford Preprint RL-75-02,RPP/H/40.

25. P. Hoyer, R.G. Roberts and D.P. Roy, Nucl.Phys. B56 (1973) 173.

26. W.F. Buhl, G. Gidal, D.F. Grether, W. Ko, M. Alston-Garnjost, A. Barbaro-Galtieri, G.R. Lynch and F.T. Solmitz, Phys.Lett.48B(1974)388.

27. D.M. Chew, M. Tabak and F. Wagner, Lawrence Berkeley Laboratory Report LBL-3396(December 1974).

28. M.G. Bowler and M.A.V. Game, Oxford Preprint(1975).

29. G. Thompson, R.C. Badewitz, J.A. Gaidos, R.L. McIlwain, K. Paler and R.B. Willmann, Nucl.Phys.B69 (1974) 381.

30. G. Otter, G. Rudolph, H Wieczorek, H. Bottcher, W. Novak, K. Bockmann, H. Plothow, V. Cocconi, M. Connihan, A. Kotanski, D. Morrison, D. Sotirou, R. Stroynowski, H. Wahl, T. Hirose and E. Leitner, Nucl.Phys.B80(1974)1.

31. A. Barbaro-Galtieri and P. Soding, in Meson Spectroscopy, C. Baltay and A.H. Rosenfeld,ed.'s, W.A. Benjamin Inc., New York, 1968, p.137.

32. W.F. Buhl, private communication.

33. B. Weinstein, G. Ascoli and L.M. Jones, Phys.Rev.D8 (1973)2904.

34. M. Ross, F.S. Henyey and G.L. Kane, Nucl.Phys.B23 (1970) 269.

35. H. Harari,Phys.Rev.Lett. 26, (1971)1400.

36. M. Jacob and G.C. Wick, Annals of Physics 7 (1959) 404.

37. J.D. Jackson, Nuovo Cimento 34 (1964) 1644.

38. B. Hyams, C. Jones, P. Weilhammer, W. Blum, H. Deitel, G. Grayer, W. Koch, E. Lorenz, G. Lütjens, W. Manner, J. Meissberger, W. Ochs, U. Steirlin and F. Wagner, Proceedings of the Conference on π-π Scattering, Tallahassee(1973) APS No.13 p.206.

39. D. Morgan, Phys.Rev. D2 (1970) 520.

40. Y. Goradia, T.A. Lasinski, M. Tabak and G. Smadja, Lawrence Berkeley Laboratory Report LBL-3011; Y. Goradia and T.A. Lasinski, Lawrence Berkeley Laboratory Report LBL-3626,submitted to Phys.Rev. D; and Y. Goradia, Lawrence Berkeley Laboratory Report LBL-3628, in preparation.

41. G. Ascoli and H.W. Wyld, Proceedings of the 4th International Conference on Experimental Meson Spectroscopy, Boston(1974) APS No.21 p.59; and G. Ascoli and H.W. Wyld, Illinois Preprint, C00-1195-309,ILL-(TH)-75-4,(February 1975).

42. I.J.R. Aitchison,"Corrections to the Isobar Model", talk given at the Daresbury Meeting on Three-Particle Phase Shift Analysis and Meson Resonance Production(1975).

Figure Captions

1. N^* pollution in the bin $1.7 \leq M_{3\pi} \leq 1.8$ GeV and $.35 \leq |t_{p\Delta}| \leq .8$ $(GeV/c)^2$. The triangles represent to the $\Delta^{++}\pi^-$ distribution and the histogram represents the $\Delta^{++}\pi^0$ distribution.

2. The moment (W_-) (see eq. 26) of the Δ^{++} decay distribution.

3. The moment (W_0) (see eq. 27) of the Δ^{++} decay distribution.

4. The moment (W_+) (see eq. 25) of the Δ^{++} decay distribution.

5. The Euler angle α with $\hat{z}$ along the π^+ for the bin $1.6 \leq M_{3\pi} \leq 1.7$ GeV and $.35 \leq |t_{p\Delta}| \leq .8$ $(GeV/c)^2$.

6. Cosine of the Euler angle β. Other specifications same as 5.

7. The Euler angle γ. Other specifications same as 5.

8. Invariant mass of the $\pi^-\pi^0$ system. Other specificatio is same as 5.

9. Invariant mass of the $\pi^+\pi^0$ system. Other specifications same as 5.

10. Invariant mass of the $\pi^+\pi^-$ system. Other specifications same as 5.

11. The experimental 3π mass spectrum for $\pi^+p \rightarrow (3\pi)^0\Delta^{++}$ as a function of $M_{3\pi}$ is given by the triangles. The left hand scale is events per 50 MeV; the right hand, μb/GeV. Fig. 11a is for $|t_{p\Delta}| \leq .35$ $(GeV/c)^2$ and Fig. 11b for $.35 \leq |t_{p\Delta}| \leq .8$ $(GeV/c)^2$. The total A_2 intensity is given by the solid circles; the ω^* intensity by the open ones. Solid cureves are Breit-Wigner fits to the 2^+ intensity at low t and to the 3^- intensity at high t. Dashed curves are the same fits

normalized to the number of events in that bin.

12. Phases relative to the T^{0+}_{20} [1(2^-S fπ)] at low t in the A_2 region. Fig. 12a is the largest unnatural parity A_2 wave, the T^{0-}_{10}[1 (2^+ D$\rho\pi$)]. Fig. 12b is the natural parity A_2 T^{1+}_{11} [1 (2^+ D$\rho\pi$)].

13. Phases relative to the T^{0+}_{20} [1(2^-S fπ)] at low t in the A_2 region. Fig. 13a is the T^{0+}_{20} [1 (0^- S$\varepsilon\pi$)]; fig.13b the T^{0+}_{20} [1(2^- D$\varepsilon\pi$)].

14. Phases relative to the T^{0+}_{20} [1(2^- D$\varepsilon\pi$)] wave as a function of $M_{3\pi}$ at high t in the ω^* region. Fig. 14a is the T^{0-}_{10} [0 (3^- F$\rho\pi$)]; fig. 14b the T^{1-}_{10} [0 (3^- F$\rho\pi$)].

15. Phases relative to the T^{0+}_{20} [1 (2^- D$\varepsilon\pi$)] at high t as a function of $M_{3\pi}$ in the ω^* region. Fig. 15a is the T^{0+}_{20} [1 (0^- S$\varepsilon\pi$)]; fig.15b the T^{0+}_{20} [1 (2^- Sfπ)].

16. The ratio of unnatural to natural exchange contributions to background as a function of $M_{3\pi}$. Fig. 16a is at low t and fig.16b is at high t.

17. The ratio of the amplitudes allowed by the quark model (s=1) those not allowed by the quark model (s=2) as a function of $M_{3\pi}$. Fig. 17a is at low t; Fig. 17b is at high t.

18. The ratio of helicity nonconserving background at the meson vertex to helicity conserving background as a function of $M_{3\pi}$. Fig. 18a is at low t and fig. 18b. is at high t.

19. The total 1^+ I=1, "A_1", intensity as a function of $M_{3\pi}$. Fig. 19a is at high t; fig. 19b at low.

20. The total 2^- I=1, "A_3", intensity as a function of $M_{3\pi}$. Fig. 20a is

at high t; fig. 20b at low.

21. The total 1^+ I=0 intensity at low t as a function of $M_{3\pi}$.

22. The total 0^- I=1 intensity as a function of $M_{3\pi}$. Fig. 22a is at high t; fig. 22b at low.

23. The total I=2 intensity as a function of $M_{3\pi}$. Fig. 23a is at low t; fig. 23b at high.

24. Differential cross sections in $\mu b/(GeV/c)^2$ for $1.2 \leq M_{3\pi} \leq 1.4$ GeV as a function of $|t_{p\Delta}|$. The histogram gives the total intensity and the plotted points give the A_2 contribution.

25. Differential cross sections in $\mu b/(GeV)c)^2$ for $1.2 \leq M_{3\pi} \leq 1.4$ GeV as a function of $|t_{p\Delta}|$. The squares give the unnatural exchange contribution to the A_2, and the diamonds give the natural exchange contribution.

26. Differential cross sections in $\mu b/(GeV/c)^2$ for $1.6 \leq M_{3\pi} \leq 1.8$ GeV as a function of $|t_{p\Delta}|$. The histogram gives the total differential cross section, while the plotted points give the ω^* contribution.

27. Differential cross sections in $\mu b/(GeV/c)^2$ for $1.6 \leq M_{3\pi} \leq 1.8$ GeV as a function of $|t_{p\Delta}|$. The squares give the natural exchange contribution to the ω^* and the diamonds give the unnatural exchange contribution.

28. Differential cross sections in $\mu b/(GeV/c)^2$ as a function of $|t_{p\Delta}|$. The points, diamonds, squares give the natural exchange contributions to ω, A_2, and ω^* production, respectively. The lines

are the results of fits to exponential functions over the monotone decreasing regions in t.

29. Differential cross sections in $\mu b/(GeV/c)^2$ as a function of $|t_{p\Delta}|$. The points, diamonds, squares give the unnatural exchange contributions to ω, A_2, ω^* production, respectively. The lines are the results of fits to exponential functions over the monotone decreasing regions in t.

30. t dependent phases in the region $1.2 \leq M_{3\pi} \leq 1.4$ GeV. Fig. 30a gives the phase between the T^{0-}_{10} A_2 and the T^{0+}_{20} [1 $(0^-\epsilon\pi)$] waves. Fig. 30b gives the relative phase between the T^{0-}_{10} and T^{1+}_{11} A_2 amplitudes.

31. Differential cross sections in $\mu b/(GeV/c)^2$ as a function of $|t_{p\Delta}|$ in the region $1.2 \leq M_{3\pi} \leq 1.4$ GeV. The points are the contributions from net helicity flip zero amplitudes in the coordinate system of the text. Fig. 31a is the T^{0-}_{10} A_2 wave. Fig. 31b is the net helicity flip zero combination of the T^{1+}_{11} and T^{1-}_{11} amplitudes.

32. Same as figure 32 except the plotted intensities are the result of crossing to the s channel helicity system.

Fig. 1: N* Pollution

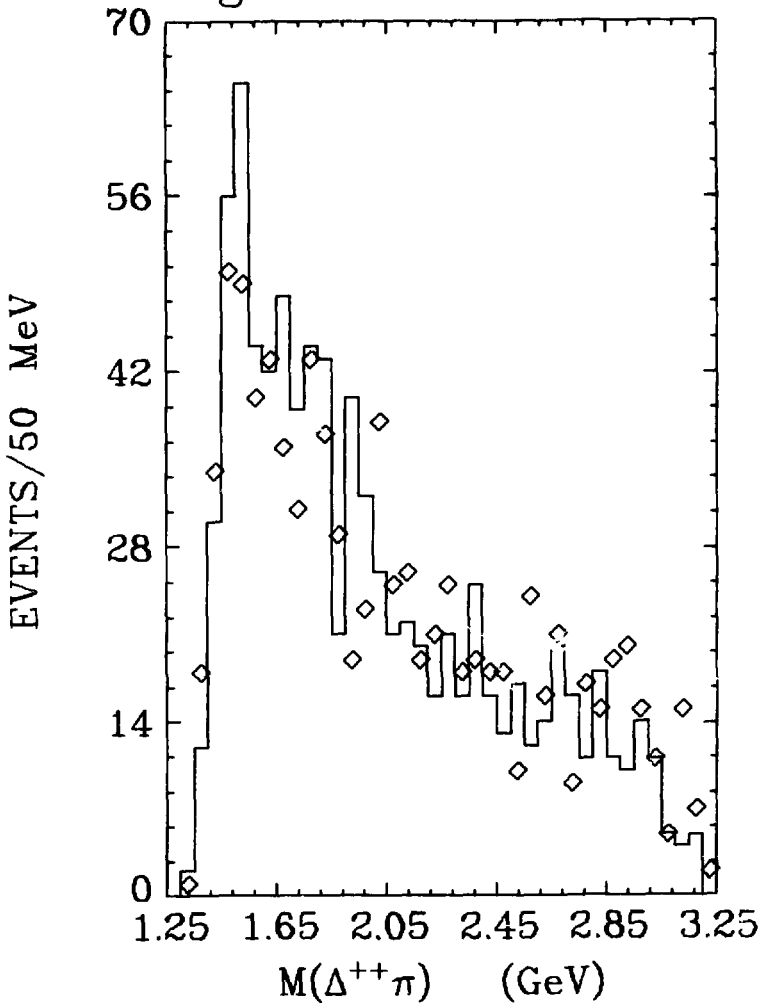

XBL 759-8142

Fig. 2: $\langle W_- \rangle$

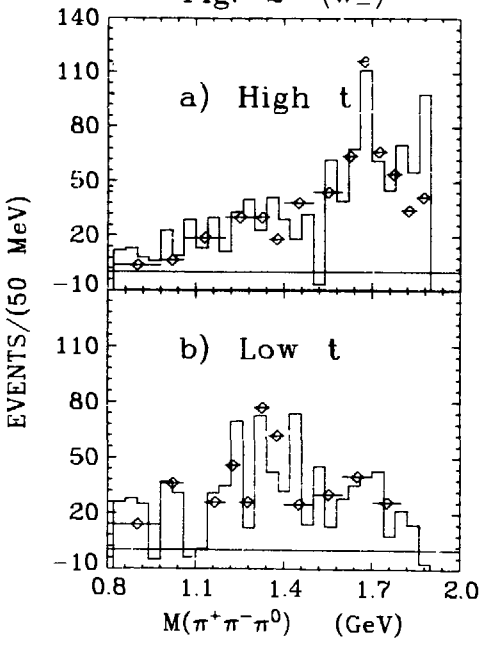

Fig. 3: $\langle W_0 \rangle$

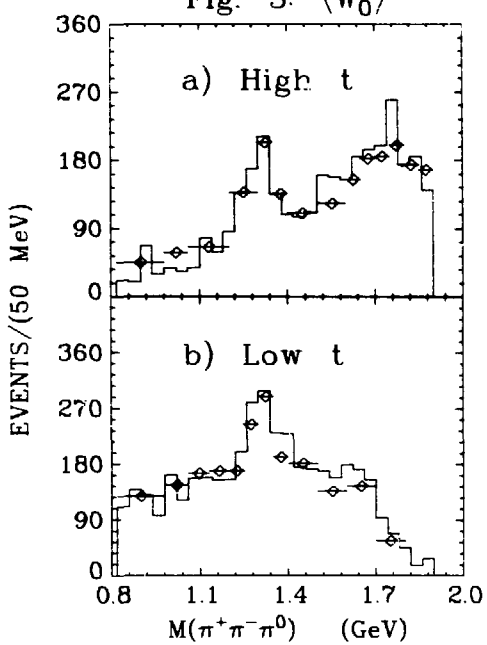

XBL 759-8144

Fig. 4: $\langle W_+ \rangle$

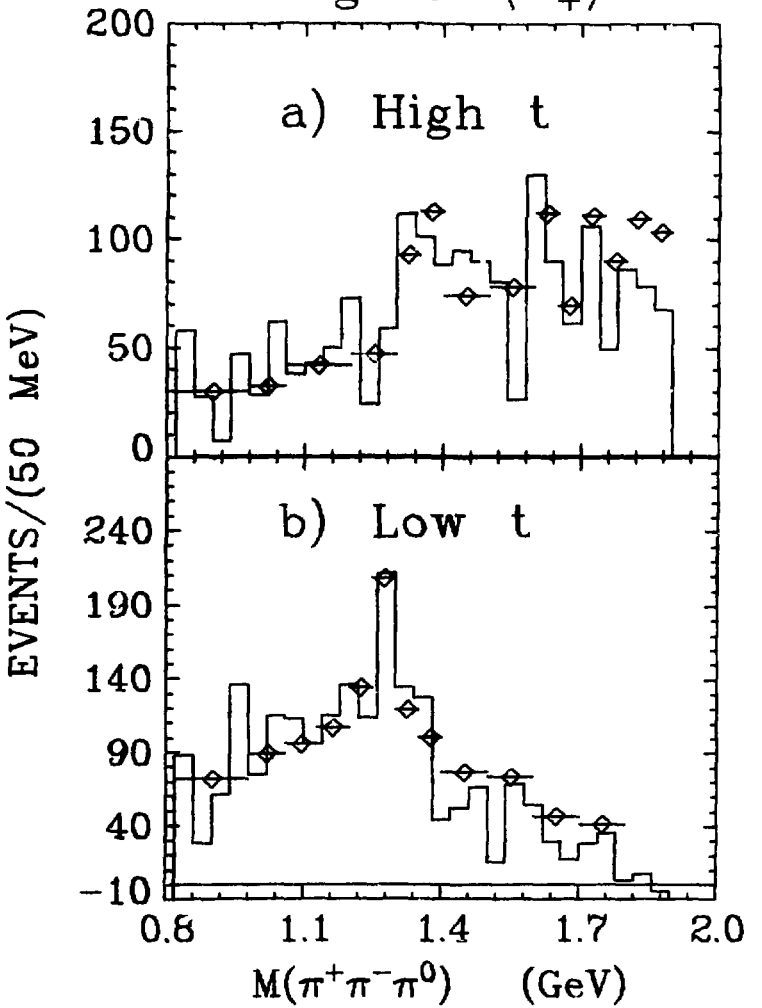

XBL 759-8143

Fig. 5

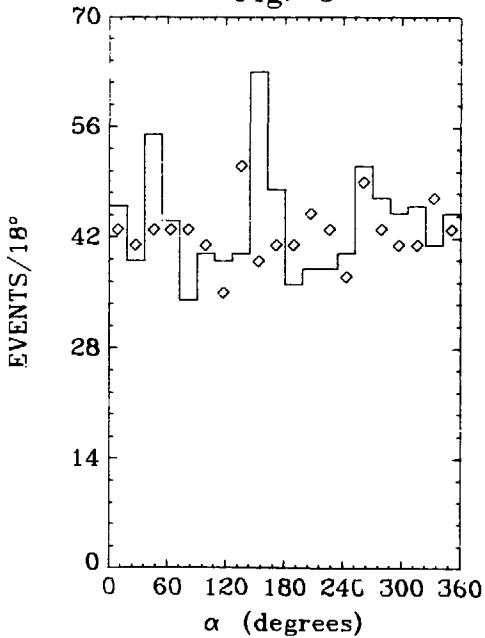

Fig. 6

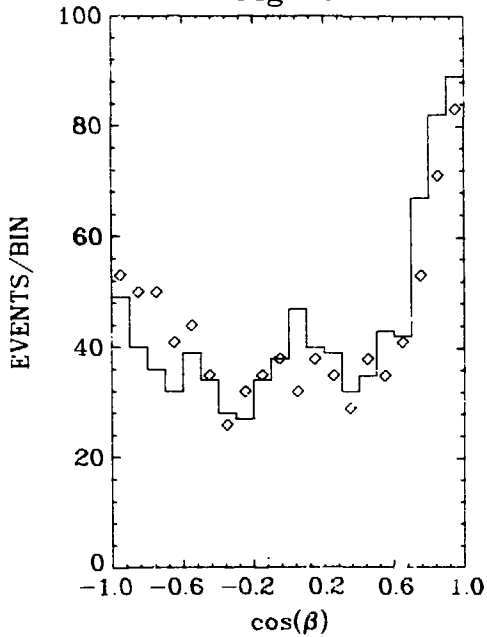

XBL 759-8158

Fig. 7

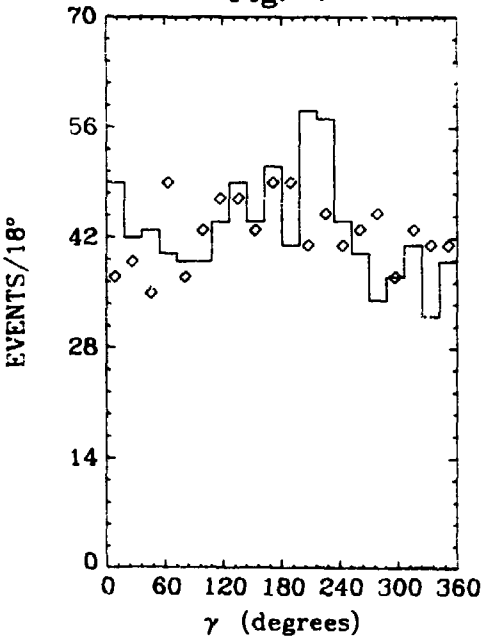

Fig. 8

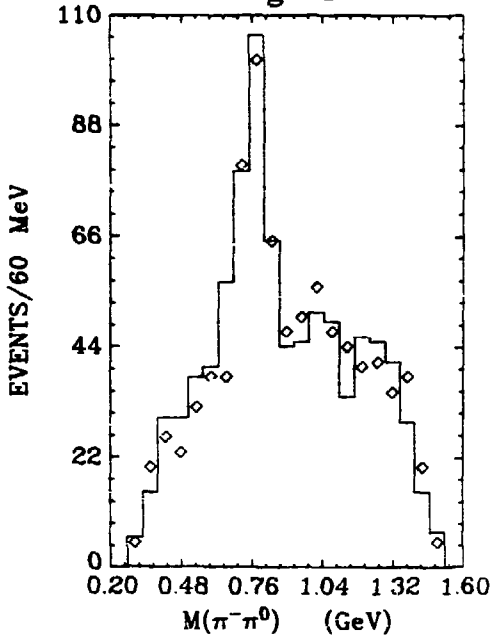

XBL 759-8157

Fig. 9

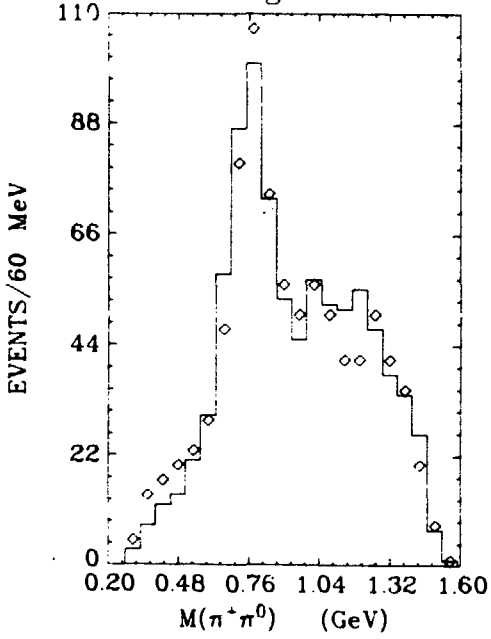

Fig. 10

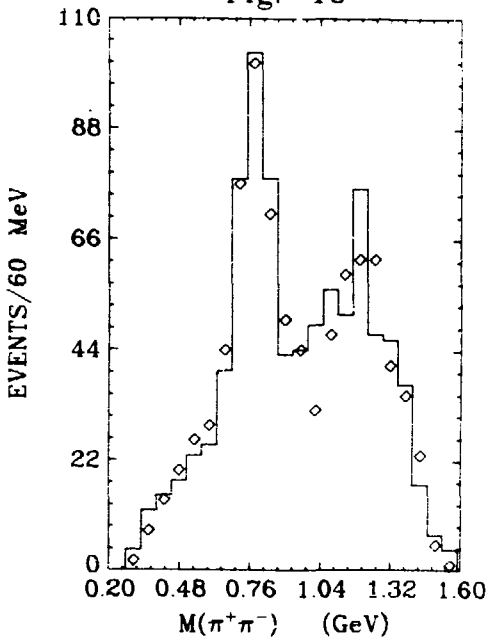

NBL 759-8156

Fig. 11

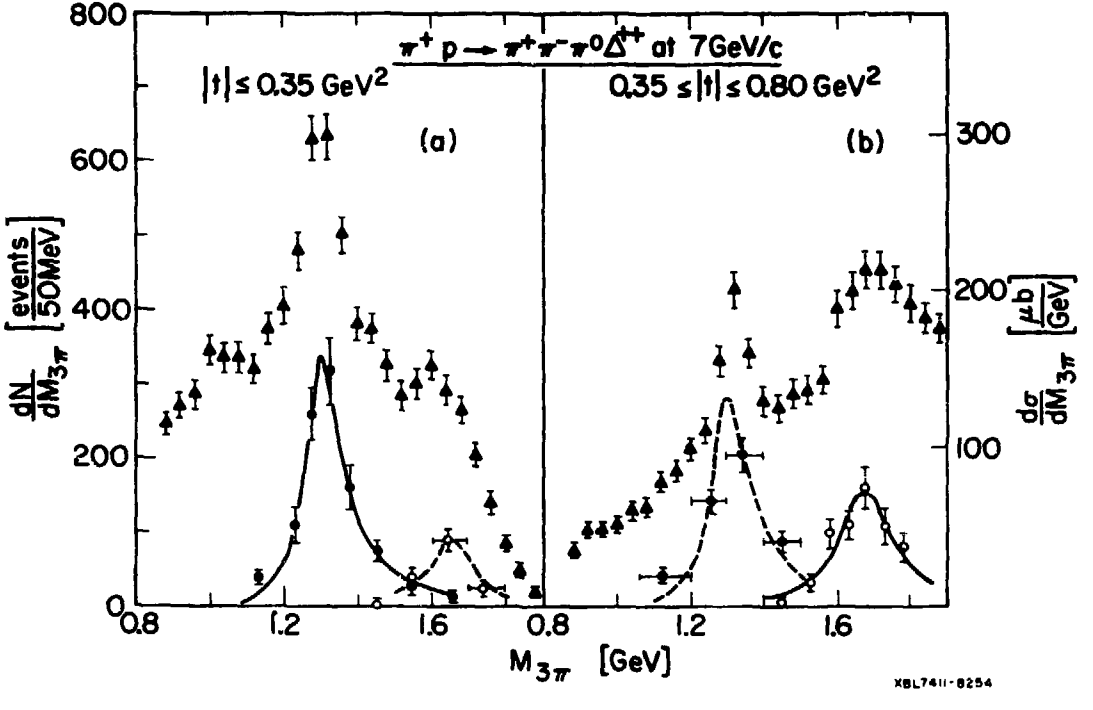
$\pi^+ p \to \pi^+\pi^-\pi^0\Delta^{++}$ at 7GeV/c
$|t| \le 0.35$ GeV^2
$0.35 \le |t| \le 0.80$ GeV^2
(a)
(b)
$\frac{dN}{dM_{3\pi}}$ [events/50MeV]
$\frac{d\sigma}{dM_{3\pi}}$ [μb/GeV]
$M_{3\pi}$ [GeV]
800
600
400
200
0
300
200
100
0.8
1.2
1.6
XBL7411-8254

Fig. 12

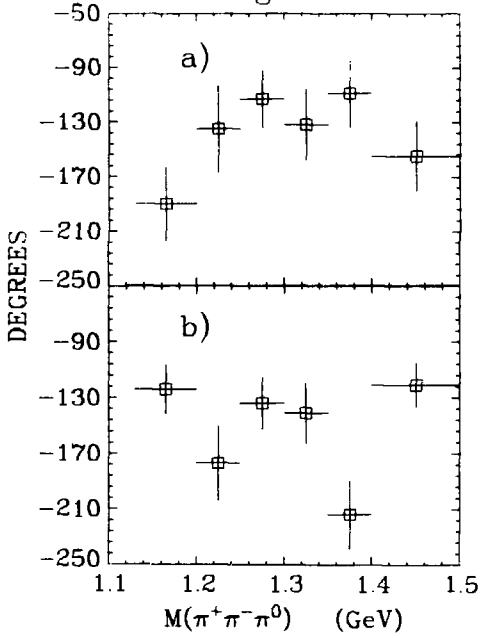

Fig. 13

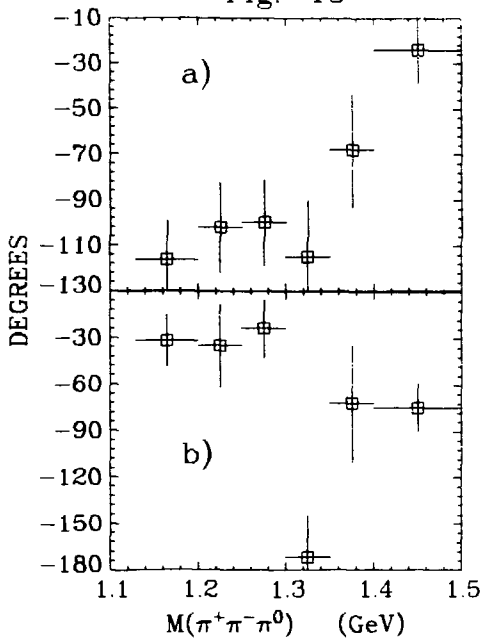

XBL 759-8155

Fig. 14

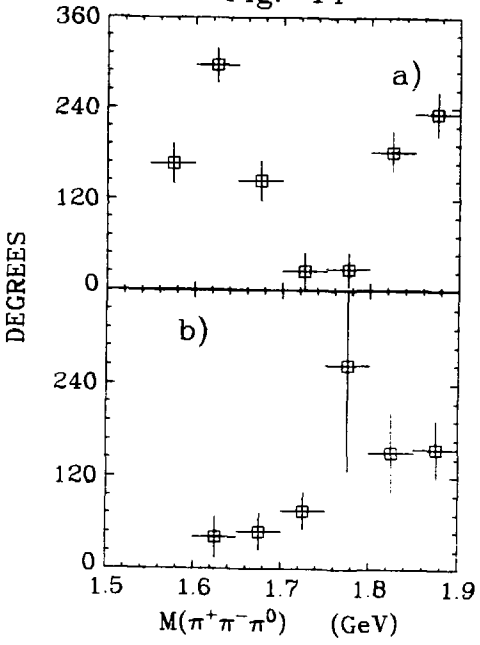

Fig. 15

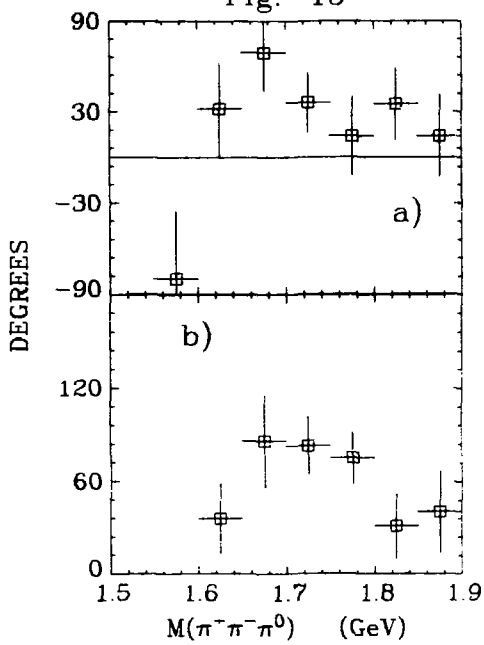

XBL 759-8154

Fig. 16

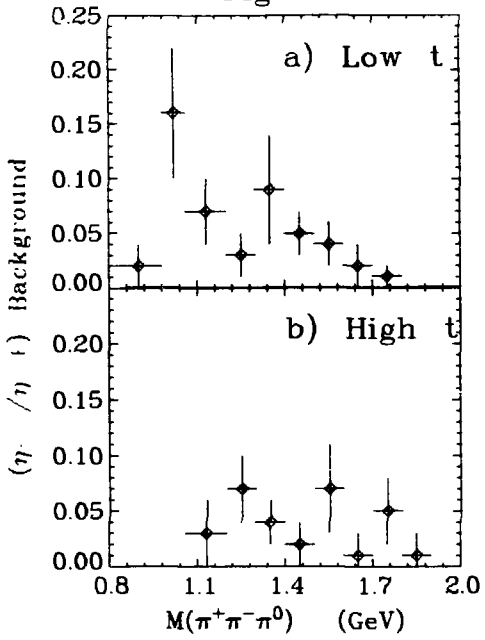

Fig. 17

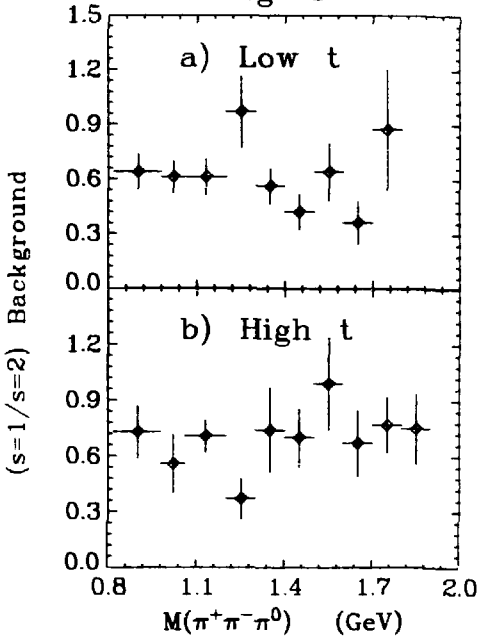

XBL 759-8153

Fig. 18

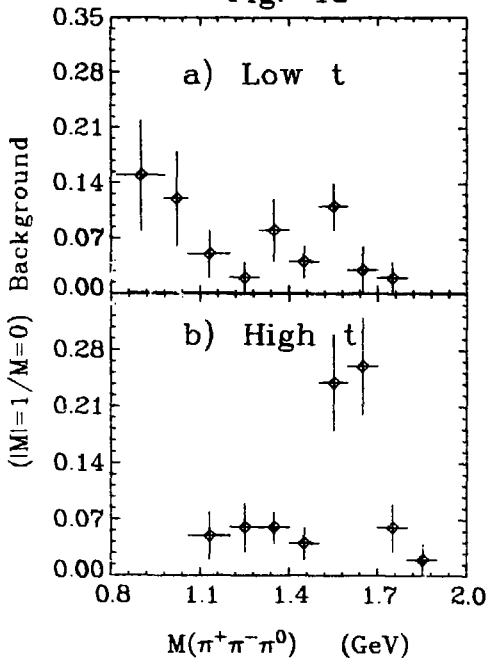

Fig. 19: A_1

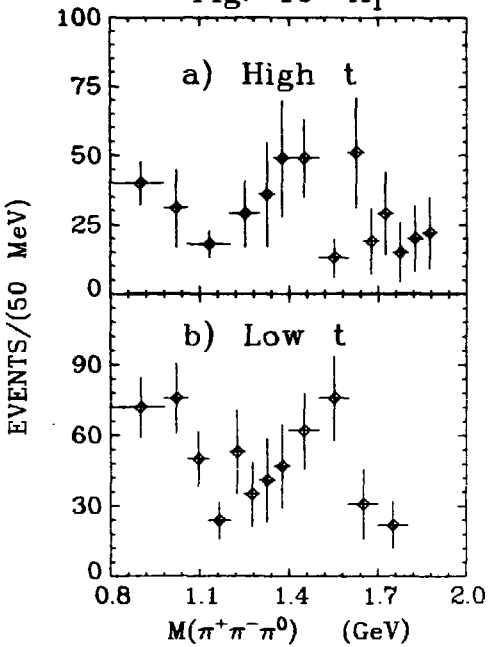

XBL 759-8151

Fig. 20: $2^-I=1$

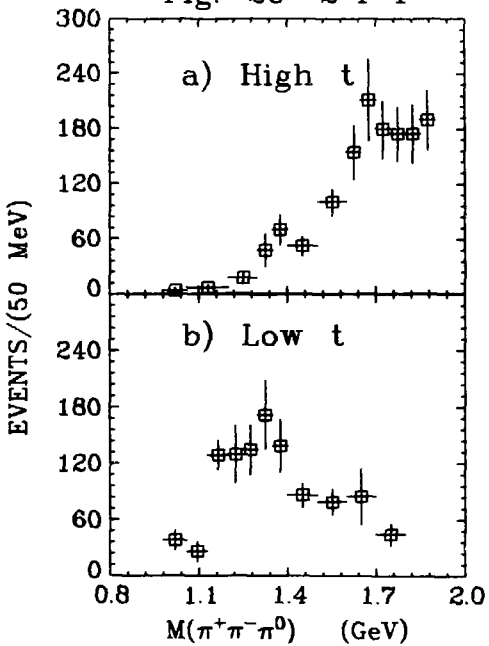

Fig. 21: $1^+I=0$

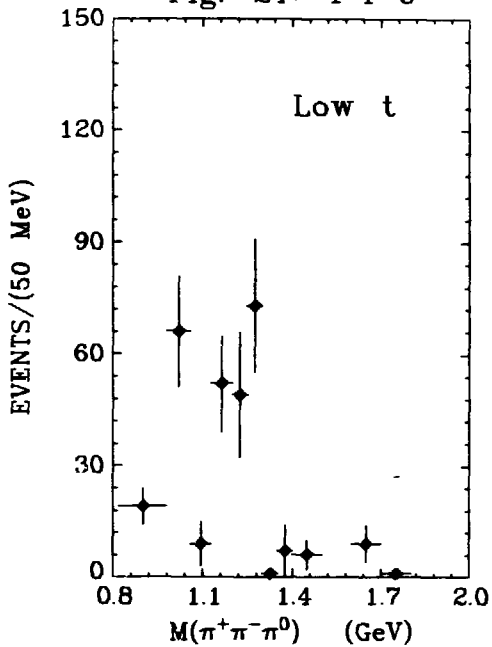

XBL 759-8152

Fig. 22: $0^-I=1$

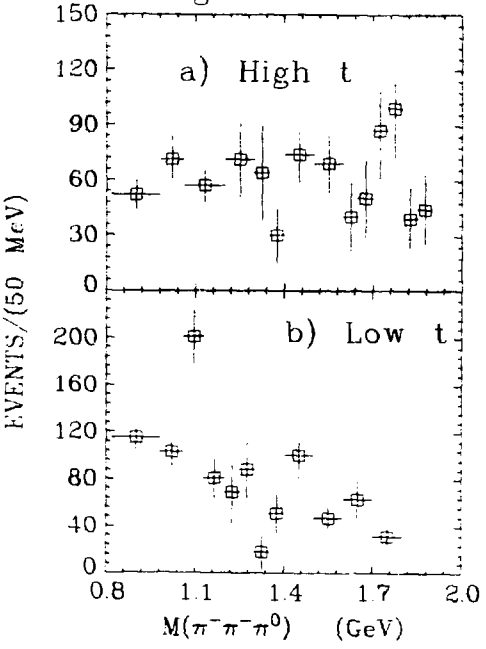

Fig. 23: Total I=2

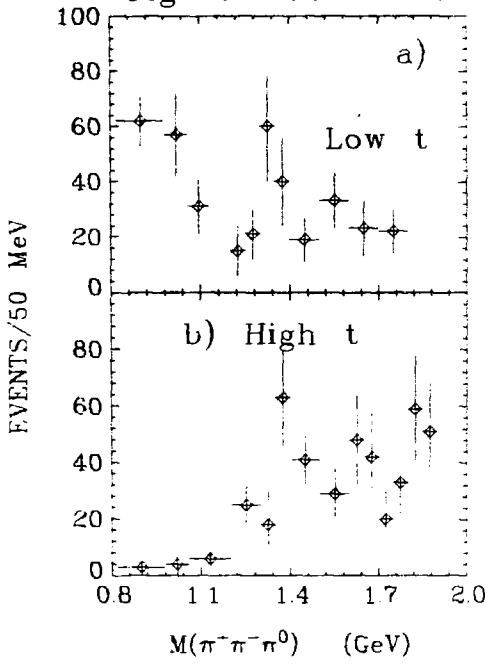

XBL 759-8149

Fig. 24: $\pi^+ p \to \Delta^{++} A_2$

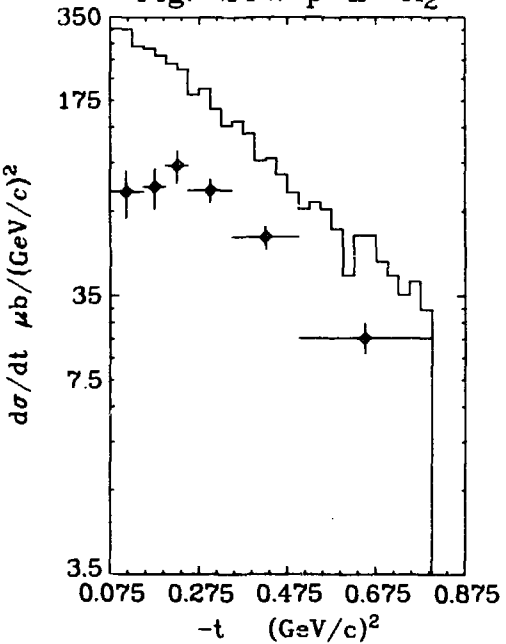

Fig. 25: $\pi^- p \to \Delta^{--} A_2$

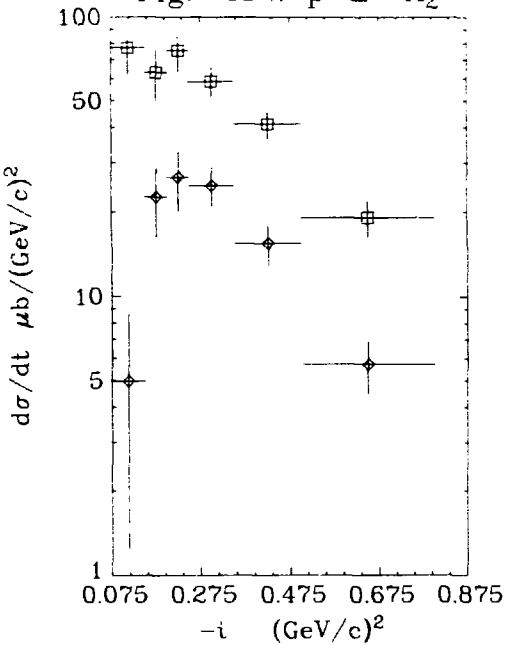

XBL 759-8150

Fig. 26: $\pi^- p \to \Delta^{++} \omega^*$

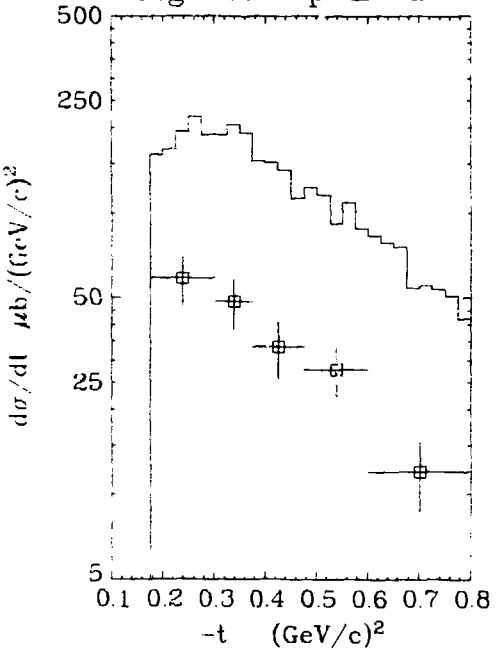

Fig. 27: $\pi^+ p \to \Delta^{++} \omega^*$

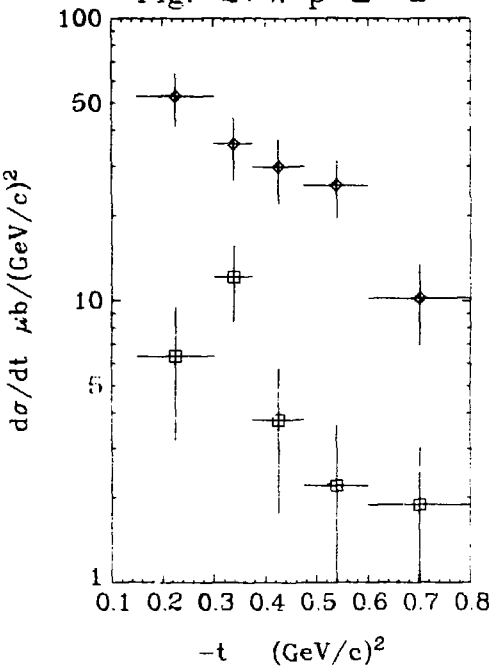

XBL 759-8148

Fig. 28

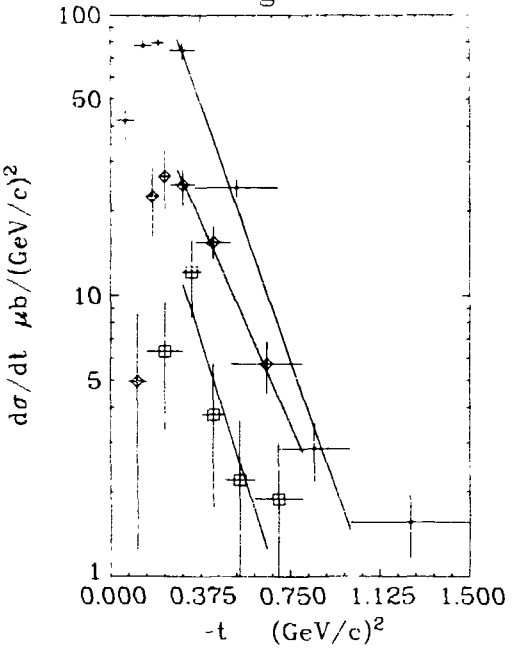

Fig. 29

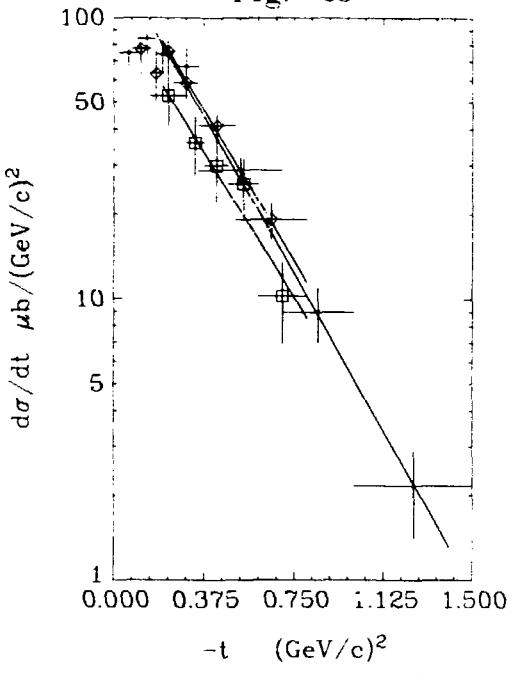

XBL 759-8147

Fig. 30: $\pi^+ p \rightarrow \Delta^{++} A_2$

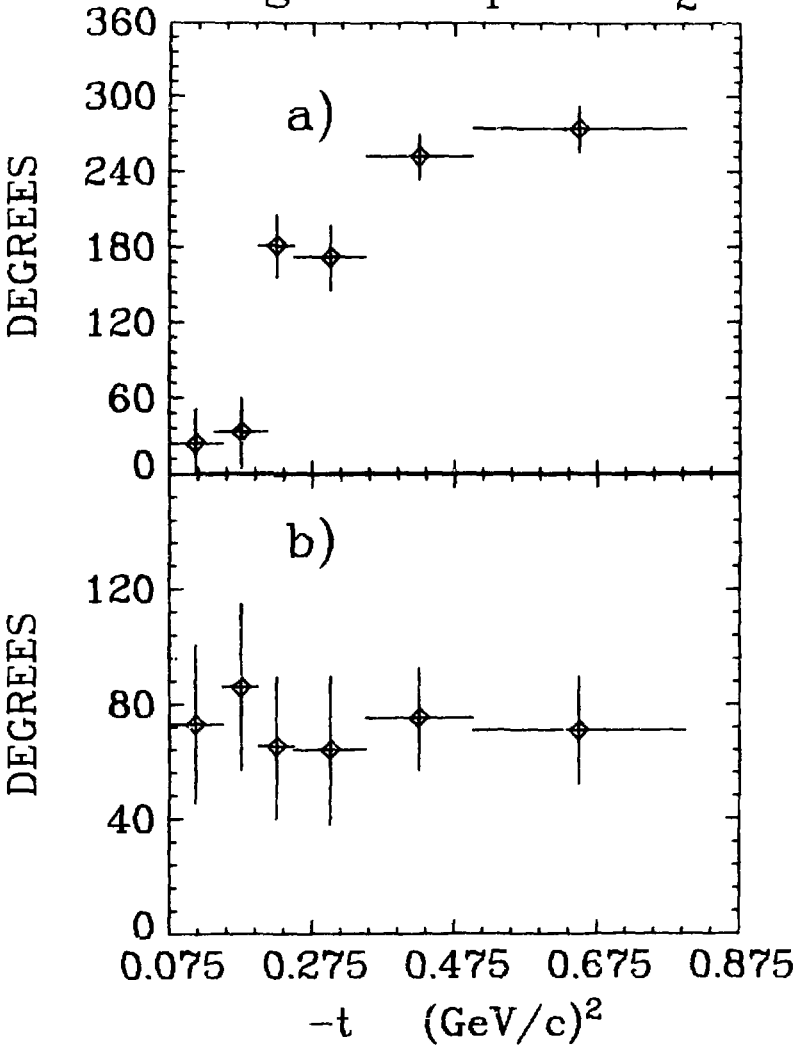

XBL 759-8146

Fig. 31

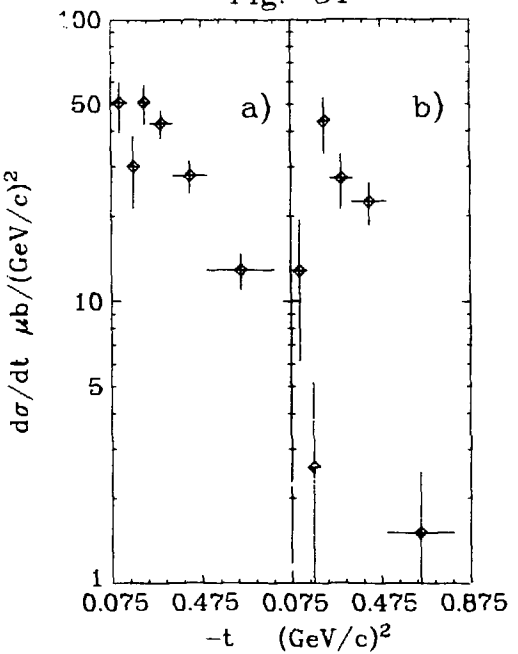

Fig. 32

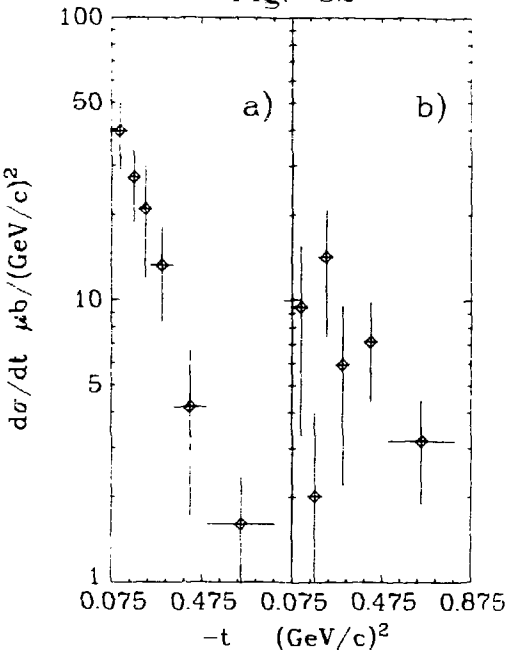

XBL 759-8145